JCB Journal of Cell Biology

ARTICLE

Astrocyte-dependent local neurite pruning in Beat-Va neurons

Katherine S. Lehmann[1], Madison T. Hupp[1], Leire Abalde-Atristain[1], Amanda Jefferson[1], Ya-Chen Cheng[1], Amy E. Sheehan[1], Yunsik Kang[1,2], and Marc R. Freeman[1]

Developmental neuronal remodeling is extensive and mechanistically diverse across the nervous system. We sought to identify *Drosophila* pupal neurons that underwent mechanistically new types of neuronal remodeling and describe remodeling Beat-Va$_M$ and Beat-Va$_L$ neurons. We show that Beat-Va$_M$ neurons produce highly branched neurites in the CNS during larval stages that undergo extensive local pruning. Surprisingly, although the ecdysone receptor (EcR) is essential for pruning in all other cell types studied, Beat-Va$_M$ neurons remodel their branches extensively despite cell autonomous blockade EcR or caspase signaling. Proper execution of local remodeling in Beat-Va$_M$ neurons instead depends on extrinsic signaling from astrocytes converging with intrinsic and less dominant EcR-regulated mechanisms. In contrast, Beat-Va$_L$ neurons undergo steroid hormone–dependent, apoptotic cell death, which we show relies on the segment-specific expression of the Hox gene *Abd-B*. Our work provides new cell types in which to study neuronal remodeling, highlights an important role for astrocytes in activating local pruning in *Drosophila* independent of steroid signaling, and defines a Hox gene-mediated mechanism for segment-specific cell elimination.

Introduction

During development, the nervous system is initially overpopulated by neurons that form an excessive number of synaptic connections. This neural circuitry is subsequently refined through the elimination of exuberant synapses, neurites, or entire neurons often in response to activity-dependent signaling mechanisms (Luo and O'Leary, 2005). While neuronal remodeling occurs in all complex metazoans and provides a mechanism for the optimization of neuronal numbers and circuit connectivity, aberrant neuronal remodeling is associated with neurological conditions like autism spectrum disorders, schizophrenia, and epilepsy (Feinberg, 1982; Selemon et al., 1995; Atz et al. 2007; Winchester et al., 2012; Sekar et al., 2016; Ishizuka et al., 2017; Neniskyte and Gross, 2017).

How much neuronal remodeling occurs across the mammalian nervous system remains unclear, but it is thought to be extensive and have profound effects on the final wiring diagram (Luo and O'Leary, 2005, Neukomm and Freeman, 2014; Riccomagno and Kolodkin, 2015). Axonal and synaptic connectivity can be radically altered through local pruning of axons or individual synaptic connections. Retinal ganglion cells (RGCs) initially project axons to the dorsal lateral geniculate nucleus (dLGN) of the thalamus and form an excessive number of synapses on target cells, but later these are refined and exuberant RGC axons and synapses are eliminated (Stevens et al., 2007; Schafer et al., 2012). Large-scale changes in circuit wiring can also be driven by selective cell death (Oppenheim, 1985; Hutchins and Barger, 1998). For instance, 40% of mouse GABAergic inhibitory neurons in the developing postnatal cortex are culled by a wave of caspase-driven cell death in the first 20 days of life (Southwell et al., 2012). Many of these changes occur long after the neurons have integrated into neural circuits and fired for weeks. Precisely how specific neurons are selected for elimination remains unclear.

Glial cells help sculpt developing neural circuits by participating in the selective elimination of neurites, synapses, or entire neurons. In the dLGN, C1q is believed to opsonize synapses that are destined for removal, and C1q-bound synapses are then recognized and phagocytosed by complement receptor 3–bearing microglia (Schafer et al., 2012). Astrocytes can also engulf pruned synapses via the MERTK and MEGF10 receptors (Chung et al., 2013), likely by also binding C1q (Iram et al., 2016; Lin et al., 2017). Disruption of C1q signaling leads to less robust RGC terminal segregation and the retention of excess functional synapses (Stevens et al., 2007), which argues that glia somehow

[1]Vollum Institute, Oregon Health & Science University, Portland, OR, USA; [2]Department of Cell and Developmental Biology, University of Colorado School of Medicine, Aurora, CO, USA.

Correspondence to Yunsik Kang: yunsik.kang@cuanschutz.edu; Marc R. Freeman: freemmar@ohsu.edu.

play a role in promoting the final execution of synapse/axon elimination rather than simply passively clearing pruned neuronal debris. However, C1q is not required in all brain areas that undergo developmental neural refinement, arguing that a diversity of pruning mechanisms exist across the brain. In the mouse barrel cortex, innervating axons are extensively refined into segregated somatosensory maps (Petersen, 2019). In this context, however, refinement relies on fractalkine signaling between neurons and microglia, and C1q signaling is dispensable (Gunner et al., 2019). Finally, it has been clear for some time that phagocytic cells, including glia, can help drive cells toward the final execution of cell death. In developing *C. elegans*, cell death requires both cell-intrinsic initiation of apoptotic pathways and signals from the engulfing hypodermal cells, with engulfing hypodermal cells signaling to partially dead cells to fully execute apoptosis (Hoeppner et al., 2001; Reddien et al., 2001). While not widely explored in the mammalian brain, similar roles for microglia have been identified in promoting the final execution of cell death in populations of developing Purkinje neurons (Marín-Teva et al., 2004). In this way, neuronal remodeling appears to entail a complex conversation between neurons and glia.

Drosophila has served as an excellent system in which to explore the molecular basis of neuronal remodeling events in vivo (Lee et al., 1999, 2000; Watts et al., 2003; Williams and Truman, 2005; Choi, 2006, Kirilly et al., 2009; Zhang et al., 2014). At pupariation, a burst of the steroid hormone 20-hydroxyecdysone (ecdysone) drives the activation of neuronal remodeling programs across the nervous system, most of which are executed during the first 12–18 h of metamorphosis (Truman et al., 1994; Schubiger et al., 1998, 2003). Ecdysone binds to the Ecdysone Receptor (EcR) nuclear hormone receptor, with EcR signaling acting as a timing mechanism to coordinate the initiation of animal-wide metamorphic changes (Pinto-Teixeira et al., 2016; Koelle et al., 1991; Riddiford and Truman, 1993; Talbot et al., 1993; Thummel, 1996). Cell-autonomous blockade of EcR signaling appears to inhibit known neuronal cell death and local pruning events in the *Drosophila* nervous system (Schubiger et al., 1998, 2003; Kuo et al., 2005; Choi, 2006; Winbush and Weeks; 2011, Hara et al., 2013; Yamaguchi and Miura, 2015; Marchetti and Tavosanis, 2017). For instance, in the first 6–8 h of metamorphosis in the central nervous system (CNS), blocking EcR signaling in ventral nerve cord (VNC) Corazonin neurons suppressed apoptotic death (Choi, 2006; Lee et al., 2011, 2013, 2019; Wang et al., 2019). Likewise, the mushroom body (MB) γ neurons in the brain, which are involved in olfactory learning and memory, undergo stereotyped axonal and dendritic pruning (Heisenberg, 1998) that can be blocked by inhibiting EcR (Lee et al., 2000; Watts et al., 2003). To our knowledge, neuronal cell types that undergo developmental remodeling independently of EcR have not been identified.

Like their mammalian counterparts, *Drosophila* glial cells play a crucial role in neuronal remodeling. Neurons become competent for remodeling when the transforming growth factor-β (TGFβ) family member Myoglianin is released from glia, which activates transcription of EcR via TGFβ receptor signaling on target neurons (Awasaki et al., 2011; Yu et al., 2013; Hakim et al., 2014; Wang et al., 2019). After cell death or neurite/synapse degeneration has occurred, glial cells act as phagocytes to recognize and phagocytose neuronal debris through conserved signaling pathways like Draper/MEGF10 (MacDonald et al., 2006; Doherty et al., 2009; Hakim et al., 2014) or Fractalkine/Orion (Boulanger et al., 2021; Ji et al., 2023; Perron et al., 2023). Whether there are other, novel mechanisms by which glial cells coordinate neuronal remodeling during metamorphosis is an open question.

A growing body of evidence implies that the signaling pathways engaged to drive neuronal remodeling are diverse and context-dependent across the brain, and we lack a deep understanding of the molecular basis of neuronal remodeling in any context (Schafer et al., 2012; Yaniv and Schuldiner, 2016; Boulanger and Dura, 2022). In this study, we sought to identify new neuronal subtypes that remodel in the *Drosophila* pupal nervous system, especially those that use novel mechanisms to regulate remodeling. We characterized two populations of neurons labeled by the *BeatVa-Gal4* driver—medial (Beat-Va_M) and lateral (Beat-Va_L) neurons—that undergo complete local neurite pruning or segment-specific apoptotic cell death, respectively. We show that local pruning in Beat-Va_M neurons can happen largely independently of EcR, but requires signaling from phagocytic astrocytes, while segment-specific cell death of Beat-Va_L neurons is downstream of EcR and governed by spatially restricted expression of the Hox gene *Abd-B*. Our work establishes Beat-Va neurons as a new model to explore neuronal remodeling in vivo and identifies new mechanisms for the regulation of developmental pruning and cell death in *Drosophila*.

Results

Beat-Va neurons undergo cell death or local pruning during metamorphosis

We wished to identify neuronal cell types that undergo developmental remodeling but use genetic programs that differ from previously characterized neurons in *Drosophila*. We, therefore, screened ∼5,500 *Gal4* lines on the open source Janelia FlyLight website (Pfeiffer et al., 2008) to identify *Gal4* driver lines that were active in sparse populations of ventral nerve cord (VNC) neurons during the wandering third instar larval stage (wL3), the developmental stage that directly precedes metamorphosis (Fig. 1 A). From these, we selected 87 lines and validated their wL3 expression patterns by crossing each line to membrane-tethered GFP (*UAS-mCD8::GFP*) (Table S1). We chose 28 lines to study further and visualized their morphologies during metamorphosis. We examined them at wL3, 6 h after puparium formation (APF) and head eversion (HE, ∼12 h APF), the time point by which most known cell types have completed remodeling, and 18 h APF (Fig. 1 A and Table S2). Among all of these lines, we chose to focus on *GMR92H04-Gal4*, which appeared to label a combination of cells undergoing cell death or local pruning.

GMR92H04-GAL4 was constructed by fusing an enhancer element for the *Beat-Va* gene to the DSCP and *Gal4* promoters (Jenett et al., 2012). We refer to this line as *BeatVa-Gal4* and the

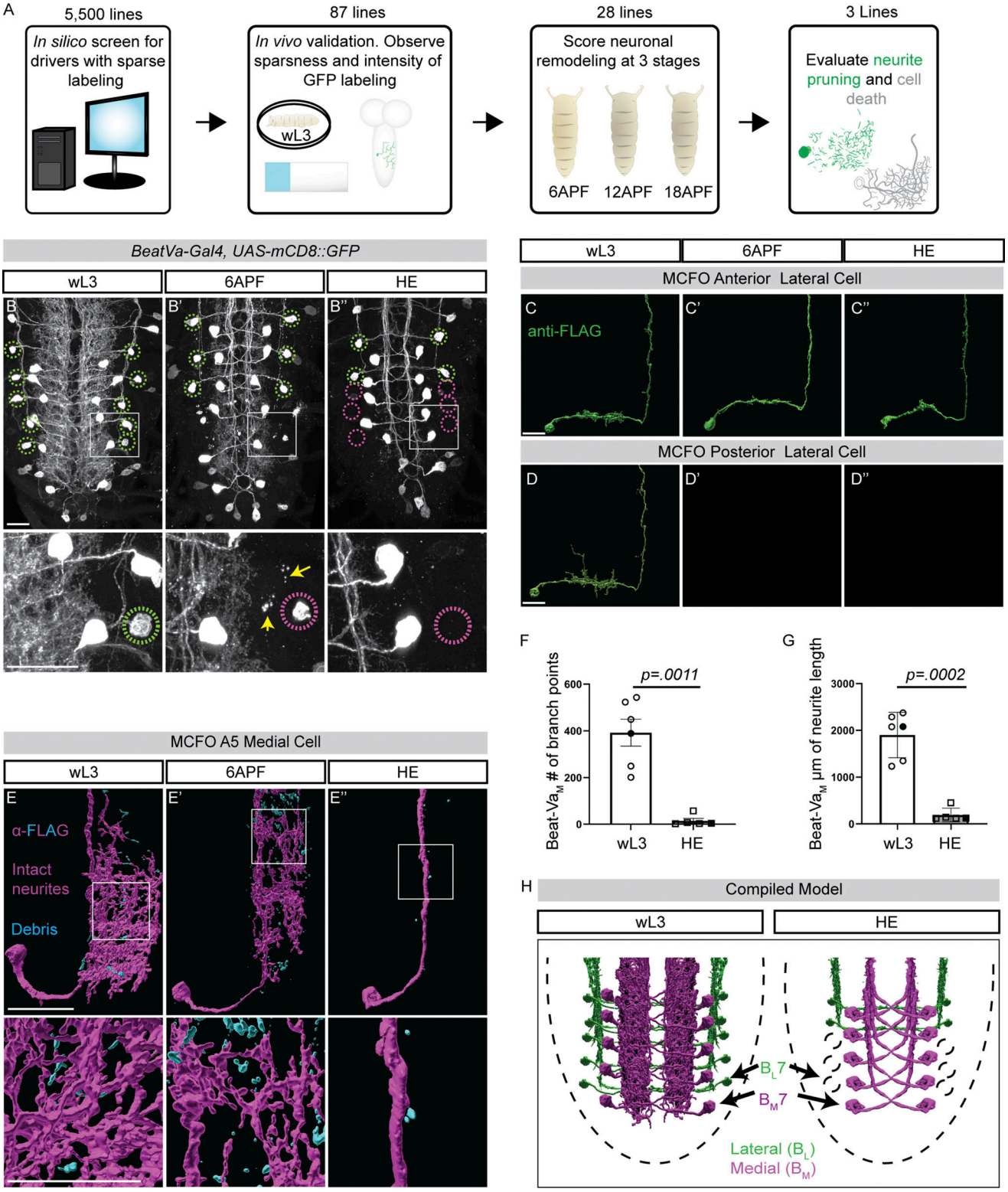

Figure 1. **Beat-Va neurons undergo local neurite pruning or cell death. (A)** *Gal4* lines generated by Janelia were screened in silico, 87 drivers that label sparse populations were verified for consistency and driver strength and 28 of those were chosen for further evaluation at 6 h APF, 12 h APF (HE), and 18 h APF. **(B–B″)** Z-projection of ventral nerve cords labeled by *BeatVa-Gal4* driving an *UAS-mCD8::GFP* transgene at wL3 (B), 6 h APF (B′), and HE (B″). Surviving lateral neurons are noted by green circles, and dead or dying lateral neurons are pink. Yellow arrows denote neurite debris. **(C–C″)** Surface rendering of single-cell morphology of the anterior Beat-Va lateral cell (Beat-Va$_L$) at wL3 (C), 6 h APF (C′), and (C″) HE. **(D–D″)** Surface rendering of posterior lateral cells at wL3 (D), 6 h APF (D′), and HE (D″). **(E–E″)** Surface rendering of Beat-Va medial cells (Beat-Va$_M$) at wL3 (E), 6APF (E′), and HE (E″). Intact neurites in magenta and fragmented neurites in cyan. **(F)** Quantification of the number of branch points in Beat-Va$_M$ cells. Error bars are SEM. **(G)** Quantification of the total combined length of all filaments in Beat-Va$_M$ cells. Error bars are SEM. **(H)** Composite model of both Beat-Va$_L$ and Beat-Va$_M$ neurons. **(F and G)** Each data point represents one cell. wL3 cells were imaged from five animals. HE cells were imaged from three animals. Comparisons by Student's *t* test. Scale bar is 20 µm. The boxed region is magnified below each panel. Colored data points correspond to the representative image shown in the figure.

neurons labeled as Beat-Va neurons. To define the segmental patterns of neurons labeled by the *BeatVa-Gal4* driver, we used antibody staining for the transcription factors Even-skipped (Eve) and Engrailed (En), which act as convenient landmarks for the identification of individual cells in the VNC (Manoukian and Krause, 1992). We found that the *BeatVa-Gal4* driver labeled one lateral neuron (referred to as Beat-Va_L) and one medial neuron (referred to as Beat-Va_M) per hemisegment in abdominal segments A3–7 (Fig. S1, A and B). This driver also weakly labeled neurons in A8 and A1–2 segments, as well as a handful of cells in the brain lobes (data not shown). The total number of cells labeled by this *BeatVa-Gal4* driver decreased prior to HE in the VNC, suggesting that a subset of neurons underwent cell death during metamorphosis. In addition, the complexity of neurite projections in the synaptic neuropil decreased significantly, indicating that some of these neurons underwent neurite pruning (Fig. 1, B and B″).

To examine the morphology of these cells in segments A3–7, we used the MultiColorFlpOut (MCFO) approach. MCFO is based on the use of UAS-regulated expression of spaghetti monster GFP transgenes (smGFP) (Nern et al., 2015). Stochastic expression of one of four UAS-regulated versions of fluorescently dead smGFP, each with a unique epitope tag (OLLAS, V5, HA, or Flag), is activated within the population of Gal4 expressing neurons (Nern et al., 2015; Viswanathan et al., 2015). Individual neurons are then visualized by staining for each epitope (Fig. S1 C). By examining single cells, we found that at the third instar larval stages, Beat-Va_L cells crossed the midline, projected anteriorly, and terminated within the VNC. Anterior Beat-Va_L neurons in segments A3–4 persisted through HE (Fig. 1 C) while posterior lateral Beat-Va_L neurons in segments A5–7 underwent cell death by 6 h APF (Fig. 1 D and Fig. S1 D). In contrast, we found that Beat-Va_M neurons extended a dense network of fine projections through multiple segments in the synaptic neuropil, totaling >1,000 µm in length. These fine processes began fragmenting by 6 h APF and were cleared from the CNS by HE (Fig. 1, E–G). These observations revealed that *BeatVa-Gal4* labels at least two cell types, one that undergoes apoptotic death and the other local neurite pruning (summarized Fig. 1 H).

Abdominal B regulates segment-specific, steroid-dependent apoptotic cell death

In all other neuronal subtypes studied to date, both neuronal cell death and local neurite pruning during *Drosophila* metamorphosis depend on neuronal ecdysone signaling (Lee et al., 2000; Kuo et al., 2005; Choi, 2006; Winbush and Weeks, 2011, Yu et al., 2013; Wang et al., 2019; Zhu et al., 2019). To determine whether ecdysone signaling also drove Beat-Va_L cell death or Beat-Va_M remodeling through EcR, we used a *UAS-EcR^{DN}* construct to cell-autonomously block EcR signaling in all Beat-Va neurons (Fig. 2, A–C). While neurite remodeling in the Beat-Va_M neurons was not disrupted by cell-intrinsic blockade of EcR signaling, expression of EcR^{DN} suppressed Beat-Va_L apoptosis (Fig. 2, A–C and E), similar to other neuronal cell death events in *Drosophila* metamorphosis (Winbush and Weeks, 2011, Denton et al., 2010; Lee et al., 2011; Zirin et al., 2013). We next stained for activated caspases using an antibody that recognized a cleaved version of Dcp-1. We found that posterior Beat-Va_L cells (A5–7) became positive for activated caspases during early metamorphosis while Beat-Va_M neurons and cells in anterior segments that survived (A3–4) were not caspase positive (Fig. S2, A–D). We then expressed P35, a baculovirus caspase inhibitor that blocks many caspase-dependent cell death events (Clem et al., 1991), using *BeatVa-Gal4*. We found that P35 had no obvious effect on Beat-Va_M remodeling, but strongly blocked Beat-Va_L cell death through HE in segments A5–6 and more weakly blocked death in A7 (Fig. 2, D and E) (perhaps due to driver strength variability), arguing posterior Beat-Va_L apoptosis is driven through caspase activation (Fig. 2, D and E; and Fig. S2).

We speculated that positional identity and segment-specific differences in survival could be regulated by differential expression of homeobox (Hox) genes. The boundary between the anterior and posterior lateral cells (A4/5) is defined by the *Abdominal-B* (*Abd-B*) Hox gene in developing embryos (Delorenzi and Bienz, 1990) and during embryonic development, Abd-B can either promote or inhibit apoptotic cell death of neuronal progenitors depending on the developmental context (Monedero Cobeta et al., 2017; Bakshi et al., 2020; Clarembaux-Badell et al., 2022). We used antibodies to determine the larval expression pattern of Abd-B and found that surviving A3–4 Beat-Va_L cells did not express Abd-B while Beat-Va_L cells in segments A5–7 strongly expressed Abd-B at wL3 and for as long as Beat-Va_L cells survived during metamorphosis (Fig. 2, F and G). We knocked down Abd-B expression specifically in the Beat-Va neurons by driving a *UAS-Abd-B^{RNAi}* construct with *BeatVa-Gal4*. This led to a strong suppression of caspase activation in posterior Beat-Va_L neurons (detected by cleaved Dcp-1 staining) through 6 h APF (Fig. S3, A–C) and partially suppressed lateral cell death compared with controls at HE (Fig. 2, H–J and L). This incomplete but strong blockade of cell death is likely due to a partial knockdown effect by the RNAi construct targeting *Abd-B* as staining for Abd-B revealed partial rather than complete knockdown of protein levels in some cells. We note that Beat-Va_L cells retained expression of EcR-B1 even when Abd-B was depleted from these cells (Fig. S3 D), arguing that the suppression of cell death could not be explained by changes in EcR expression. When we performed the reciprocal experiment and expressed Abd-B in all Beat-Va_L neurons by driving *UAS-Abd-B* with *BeatVa-Gal4* (Fig. S3 E), we found that A3–A4 lateral cells underwent cell death by HE (Fig. 2, K and L), indicating that expression of Abd-B in Beat-Va_L neurons is sufficient to induce cell death during metamorphosis. Finally, we note that Beat-Va_M neurons also expressed Abd-B, but manipulations had no effect on cell survival or neurite pruning, indicating Abd-B promotes caspase activation in some but not all neurons during metamorphosis (Fig. 2, H–K; and Fig. S3, F and G).

Local pruning in Beat-Va_M neurons is not driven by EcR

It was surprising that EcR manipulations had no obvious effect on Beat-Va_M neurite pruning, as signaling through EcR-B1 drives most neuronal remodeling during *Drosophila* metamorphosis. One possibility was that Beat-VaM neurons do not express EcR-B1 and are therefore unaffected by EcR manipulations; however, we found EcR-B1 was indeed expressed in Beat-Va_M neurons in

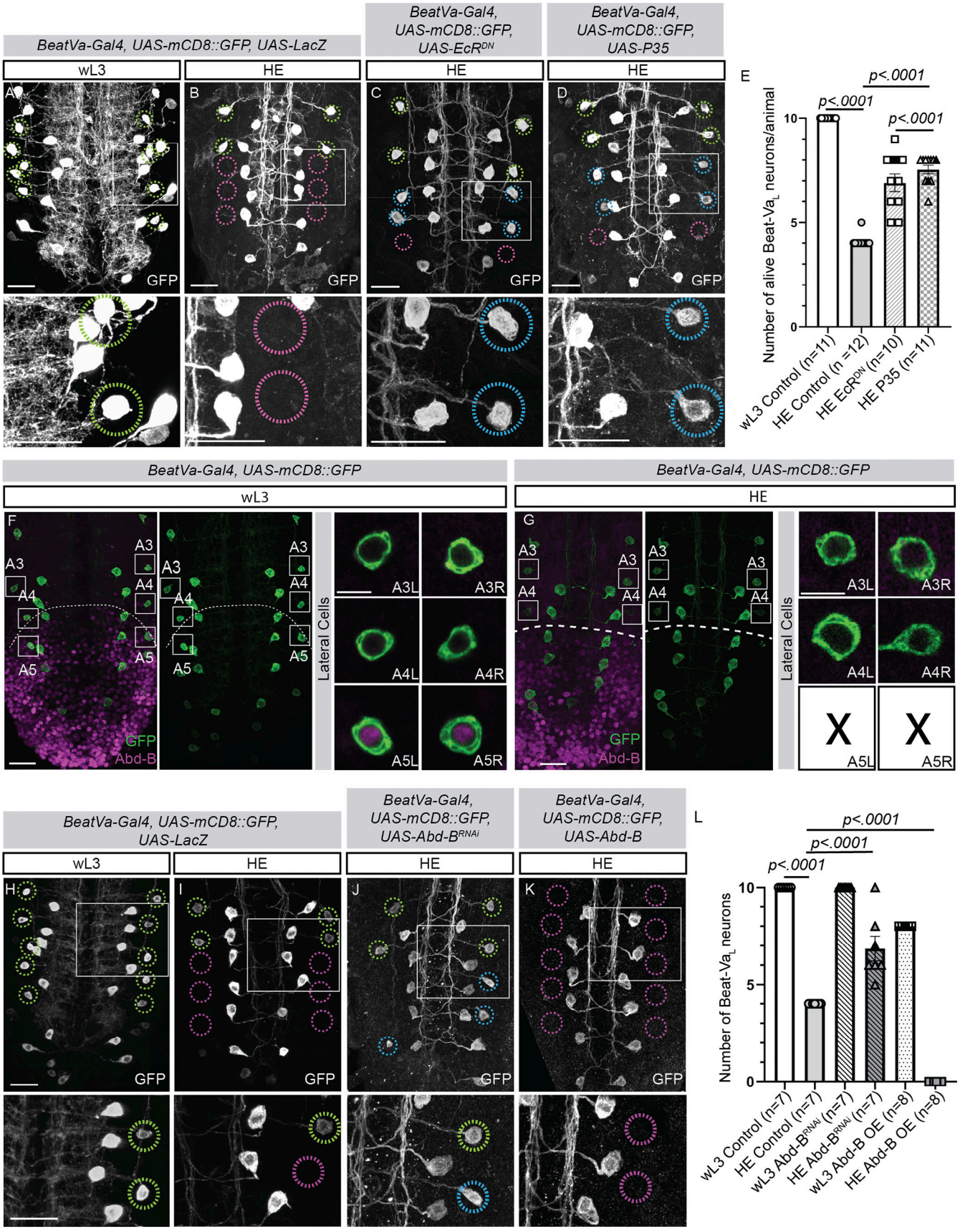

Figure 2. **Beat-Va$_L$ neurons undergo hormone-dependent, caspase-activated, Hox gene–mediated apoptosis. (A and B)** Beat-Va neurons at wL3 (A) and HE (B) were genetically labeled with mCD8::GFP expressing *UAS-LacZ* (control). **(C and D)** Beat-Va neurons at HE expressing mCD8::GFP with EcR^{DN} (C) or *UAS-*

P35 (D). Lime green circles indicate normal lateral cells before remodeling. Pink circles indicate the position of dead lateral cells. Blue circles indicate lateral cells surviving beyond the normal time point. Scale bars, 20 µm. **(E)** Quantification of the number of lateral cells at wL3, or HE in controls, or animals expressing EcR^{DN} or P35. Two-way ANOVA, Sidak multiple comparison test. *N* = number of animals. **(F and G)** Beat-Va neurons at (F) wL3 or (G) HE labeled with mCD8::GFP stained with Abdominal-B antibody (magenta). White dashed line denotes the boundary of the Abd-B expression. **(H and I)** Beat-Va neurons at wL3 (H) or HE (I) genetically labeled with mCD8::GFP crossed to *UAS-LacZ* as a control. Green circles indicate Beat-Va_L neurons. Magenta circles, the position of dead cells. **(J)** Expression of *UAS-Abd-*B^{RNAi} in Beat-Va neurons. Blue circles, cells that survive ectopically. **(K)** Expression of Abd-B in all lateral cells by HE leads to cell death. **(L)** Quantification of E–H. Two-way ANOVA, Sidak test for multiple comparisons. *n* = number of animals. **(A–G)** Scale bars are 20 µm in population images and 5 µm in the magnified view. **(H–K)** Scale bars are 20 µm. Colored data points correspond to the representative image shown in the figure. All error bars are SEM.

segments A3–7 (Fig. S3 H). To visualize individual cells more precisely in the context of EcR signaling manipulations, we generated single-cell clones in Beat-Va_M neurons and quantified neuronal complexity in wL3 stages and HE using the MCFO approach. At wL3 stages, we found no differences in Beat-Va_M neuron morphology and neurite complexity when we compared controls with EcR^{DN} expressing cells, regardless of the segment (A3–7), arguing that EcR^{DN} expression throughout larval stages does not alter Beat-Va_M neuron development (Fig. 3, A–F). We also confirmed that expression of EcR^{DN} did not block local pruning of Beat-Va_M neurites by HE (Fig. 3, A–F), as measured by total neurite length or total number of branch points (Fig. 3, E and F).

We sought to explore the possibility that EcR^{DN} could be failing to block pruning due to insufficiently high levels of expression in Beat-Va_M neurons. We first stained for the EcR^{DN} protein and observed robust expression of EcR^{DN} in all Beat-Va_M neurons at 6 h APF when endogenous EcR levels are low (Fig. S3 I). It was also possible that EcR^{DN} might have sufficient inherent activity to induce pruning in Beat-Va_M neurons (Cherbas et al., 2003), so we devised alternative strategies to block EcR signaling. Because *EcR* mutants are lethal at late embryonic or early larval stages and the *EcR* locus is proximal to FRT sites used for mosaic analysis, we used CRISPR/Cas9 technology to selectively eliminate genes required for EcR signaling in Beat-Va neurons (Meltzer et al., 2019). Briefly, we used lines that ubiquitously express guide RNAs (gRNAs) to *EcR*, its obligate heterodimer, *ultraspiracle* (*usp*) (Yao et al., 1993), or *plum*, an IgSF molecule that activates *EcR* transcription (Yu et al., 2013), and then expressed *UAS-Cas9* selectively in Beat-Va neurons with *Beat-Va-Gal4*. Targeting *EcR* and *plum* using gRNAs/Cas9 led to a significant reduction in EcR expression as expected, while targeting *usp* did not change EcR expression (Fig. S3, J and K). When we examined the refinement of Beat-Va_M neurons at HE, we observed only minor preservation or regrowth of small projections in *usp*, *EcR*, and *plum* gRNA backgrounds (Fig. 3, G–N). We observed a similar small degree of neurite preservation when Cas9-mediated knockout of Rpn6 was induced in Beat-Va_M neurons (Fig. 3, O and P), suggesting that EcR-dependent pruning in these cells occurs through the ubiquitin-proteasome system (UPS), as shown previously in MB γ neurons (Watts et al., 2003; Hoopfer et al., 2008). Although caspase activation can drive neurite pruning in other populations of neurons, expression of P35 in Beat-Va_M neurons did not block their pruning (Fig. 2 D). Moreover, cleaved Dcp-1, an activated caspase, was not present either in Beat-Va_M cell bodies from wL3 to 6 h APF—the time at which Beat-Va_M neurons remodel (Fig. S2, A–D). We wondered if, alternatively, Beat-Va_M neurons might use axon injury signaling to prune neurites. To test this, we used a *Gal4* to express Wallerian degeneration slow (WldS), which potently blocks axon degeneration after injury (Mack et al., 2001), and this had no effect on Beat-Va_M neuron pruning (Fig. 3, Q and R). Together these data suggest that Beat-Va_M neurons activate local pruning in a manner that does not depend on caspases or injury signaling and that the minor role we can detect for EcR occurs through the UPS pathway.

Finally, to examine single-cell morphology in a strong EcR depletion condition we used MCFO in combination with RNAi to concurrently knock down *BaboA* and *plum*, two transmembrane proteins that work together to induce EcR transcription, using UAS-driven RNAi constructs in *BeatVa-Gal4* animals (Fig. 4, A–D) (Zheng et al., 2003; Yu et al., 2013; Wang et al., 2019). This strategy caused a strong depletion of EcR protein as determined by antibody stains (Fig. 4 E), but we found Beat-Va_M neurons still successfully pruned their neurites (Fig. 4, F–K). These data, coupled with our observations using EcR^{DN} and gRNAs/Cas9, support the notion that neurite pruning in Beat-Va_M neurons occurs largely independently of neuronal EcR signaling.

Local pruning in Beat-Va_M neurons is not altered by manipulating neuronal activity

Recent work has shown that neuronal activity plays a role in MB γ neuron remodeling, with silencing or activating neuronal activity disrupting pruning (Mayseless et al., 2023). To determine whether neuronal activity might play a similar role in Beat-Va_M neurons, we first inhibited activity by expressing the human version of Kir2.1, an inwardly rectifying K+ channel that causes hyperpolarization, using *UAS-Kir2.1* (Baines et al., 2001). We found that Beat-Va_M neuronal morphology and pruning were normal at the wL3 and HE stage (Fig. 5, A–D). To explore the possibility that increasing neuronal activity might disrupt pruning, we expressed TrpA1, a temperature-sensitive cation channel that is inactive at 25°C but active at 29°C (Hamada et al., 2008) in Beat-Va_M neurons. We shifted them to 29°C during the first 12 h of metamorphosis, similar to the manipulation that alters MB γ neuron remodeling (Mayseless et al., 2023), or more chronically by raising the animals at 29°C for 48 h prior to HE. Neither manipulation had any effect on Beat-Va_M neuron pruning (Fig. 5, E–L) Taken together, these data argue against the notion that neuronal activity plays a significant role in Beat-Va_M local pruning.

Astrocytes non-cell-autonomously regulate Beat-Va_M neuron pruning

Beat-Va_M neurite fragmentation and clearance occur during the EcR-dependent transformation of larval astrocytes into

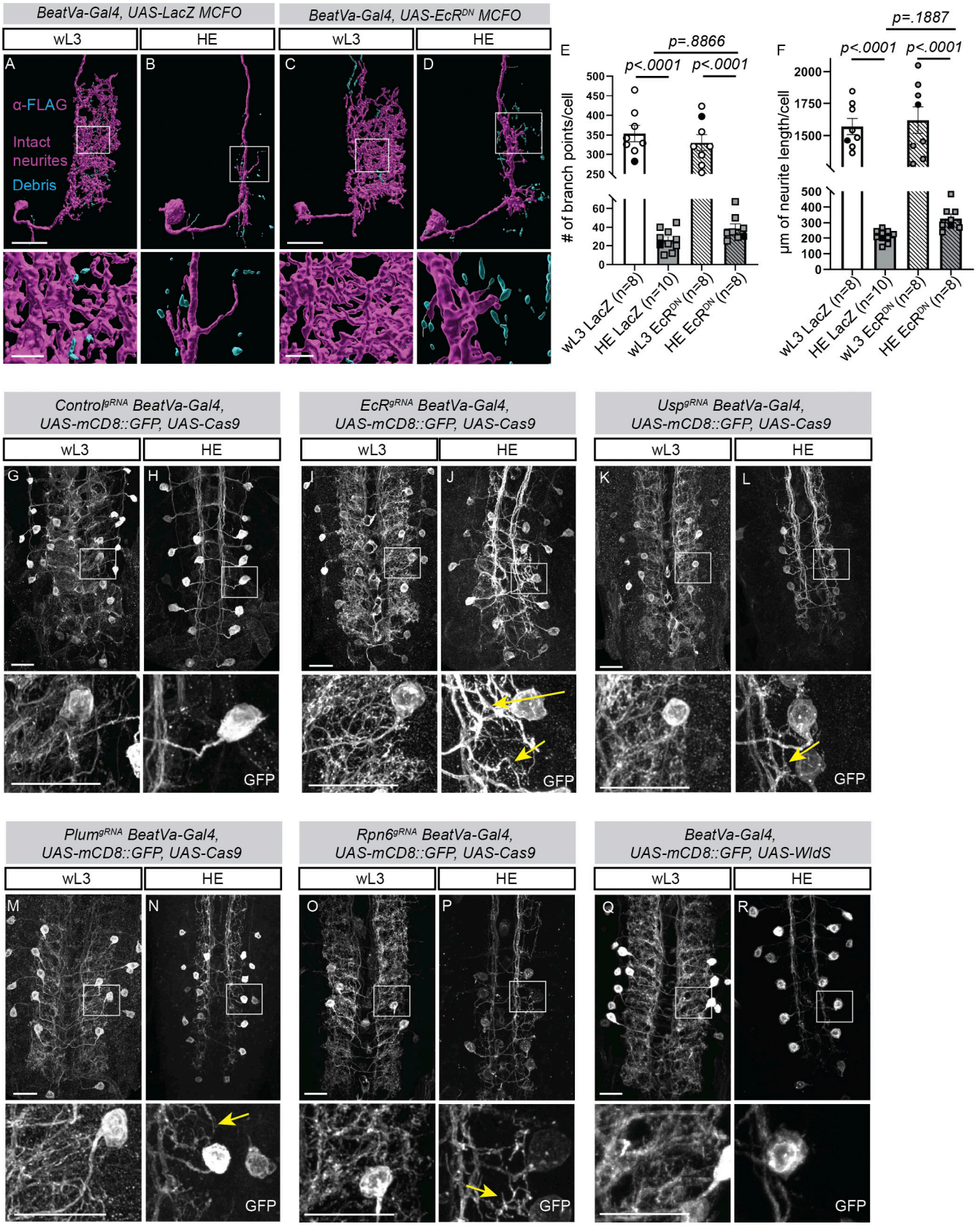

Figure 3. **Beat-Va$_M$ neurons remodel when neuronal EcR signaling or expression is inhibited. (A and B)** Surface rendering of control Beat-Va$_M$ neuron driving *UAS-LacZ* using the MCFO technique at wL3 (A) and HE (B). Intact neurites, magenta; fragmented neurites, cyan. Boxed area is shown in high magnification below each image. **(C and D)** Beat-Va$_M$ neuron expressing EcR^{DN} labeled with the MCFO technique at wL3 (C) and HE (D). **(E)** Quantification of Beat-

Va_M branch point number at HE in EcR^{DN} background. **(F)** Quantification of Beat-Va_M total neurite length in EcR^{DN} background. **(G and H)** Beat-Va neurons genetically labeled with mCD8::GFP and expressing Cas9 under UAS control. gRNAs are expressed ubiquitously. Cell-specific knockout of control gRNAs at wL3 (G) and HE (H). **(I and J)** Targeting *EcR* with gRNAs in $Beat_M$ neurons at wL3 (I) or at HE (J). Fine neurites, yellow arrow. Boxed areas are displayed in high magnification below each image. **(K and L)** *usp* gRNAs in $Beat_M$ neurons at wL3 (K) or HE (L). Fine neurites, yellow arrow. **(M and N)** Expression of *plum* gRNAs in wL3 neurons (M) and HE (N). Fine neurites, yellow arrow. **(O and P)** Expression of *Rpn6* gRNAs in wL3 neurons (O) and HE (P). Fine neurites, yellow arrow. **(Q and R)** Expression of *UAS-WldS* in wL3 neurons (Q) and HE (R) does not change Beat-Va_M neurite pruning. Comparisons with two-way ANOVA and Sidak test for multiple comparisons. **(G–R)** Scale bars are 20 µm. **(A–D)** Scale bars are 20 µm in single cell images and 5 µm in the magnified view. **(E and F)** Each data point represents one cell. For wL3 LacZ cells were imaged from seven animals, for HE LacZ cells were imaged from five animals, for wL3 EcRDN cells were imaged from eight animals, for HE EcRDN cells were imaged from five animals. **(G–R)** At least seven animals were examined per genotype and timepoint. Colored data points correspond to the representative image shown in the figure. All error bars are SEM.

phagocytic glia (Tasdemir-Yilmaz and Freeman, 2014; Yunsik et al., 2023, *Preprint*). To determine what role astrocytes might play in driving Beat-Va_M neuron remodeling, we generated a *LexAop-EcR^{DN}* line which we could drive with *alrm-LexA* to selectively block the transformation of astrocytes into phagocytes while allowing all other EcR-mediated neuronal signaling events to proceed normally. We first confirmed that our *LexA/LexAop* constructs efficiently blocked astrocyte transformation into phagocytes at HE. Indeed, expression of this *LexAop-EcR^{DN}* construct in astrocytes resulted in astrocytes retaining their bushy larval morphology, much like what we observe with the established, UAS-driven version of EcR^{DN} (Fig. S4, A–J) (Hakim et al., 2014; Tasdemir-Yilmaz and Freeman, 2014). We then used the MCFO approach to examine Beat-Va_M neuron architecture at wL3, 6 h APF, and HE after blocking EcR signaling selectively in astrocytes. Strikingly, we found that blockade of EcR signaling in astrocytes strongly suppressed local pruning of Beat-Va_M neurons to HE, where we observed significantly less neurite remodeling in Beat-Va_M neurons (Fig. 6, A–F).

Given that inhibition of EcR signaling in Beat-Va_M neurons had a small effect on local pruning, we speculated that the remodeling of Beat-Va_M neurons might be driven by a combination of EcR signaling in Beat-Va_M neurons and astrocytes synergistically. To test this directly, we blocked both astrocyte and neuronal ecdysone signaling by driving a *UAS-EcR^{DN}* simultaneously in both astrocytes and Beat-Va neurons (using *alrm-Gal4* and *BeatVa-Gal4*). We found that the combination of blocking astrocyte transformation and blocking neuronal ecdysone signaling led to a complete inhibition of local pruning in Beat-Va_M neurons (Fig. 6, G–L; and Fig. S4, K–N). Together, these data, coupled with those above, indicate that local Beat-Va_M neurite pruning occurs in response to EcR-dependent signaling in both Beat-Va_M neurons and astrocytes, with astrocytic EcR signaling playing the primary role. Finally, we note that at wL3 stages before local pruning of Beat-Va_M neurons, neurites in animals expressing astrocytic EcR^{DN} were less elaborate compared with controls, with a small decrease in total neurite length and number of branch points (Fig. 6, E, F, K, and L). This observation argues that EcR-dependent signaling in astrocytes is important for a small fraction of Beat-Va_M neurite growth during embryonic or larval stages.

The TGFβ molecule Myoglianin (Myo) activates EcR expression in astrocytes to drive Beat-Va_M neuron local pruning

In previously studied *Drosophila* neuronal subtypes, pan-glial release of the TGFβ molecule Myo, which signals through the two TGFβ receptors BaboA and Plum, results in upregulation of EcR in neurons so they are competent to remodel in response to ecdysone (Awasaki et al., 2011; Yu et al., 2013). RNAi knockdown of Myo in all glia using *repo-Gal4* suppresses the remodeling of these neurons in the *Drosophila* CNS (Awasaki et al., 2011). Although our data suggested that EcR signaling plays only a minor role in Beat-Va_M remodeling, we wanted to explore the possibility that astrocytic Myo might be the factor regulating Beat-Va_M neuron pruning, perhaps through an EcR-independent mechanism. We first generated a *BeatVa-LexA* line and drove *LexAop-CD4-tdGFP*, a membrane-targeted GFP (Poe et al., 2017), and co-expressed it with *UAS-Myo^{RNAi}* in glia. We also confirmed the fidelity of the *BeatVa-LexA* line by comparing its overlap with *BeatVa-Gal4, UAS-mCD8::cherry* (Fig. S5). When we drove the expression of *Myo^{RNAi}* in all glia, we observed a strong suppression of Beat-Va_M neuron local pruning compared to controls (Fig. 7, A–D). However, when we drove *Myo^{RNAi}* only in astrocytes or only in cortex glia, it did not affect Beat-Va_M neuron local pruning (Fig. 7, E and F). Thus, blockade of Myo signaling from all glia, but not astrocytes alone, can block Beat-Va_M neuron neuronal remodeling.

Given our data demonstrating the importance of astrocytic EcR signaling for Beat-Va_M pruning, we explored the possibility that pan-glial Myo knockdown could disrupt EcR activation in astrocytes. Previous work on MB pruning has shown that Myo is released in a redundant manner from all glia to drive the upregulation of neuronal EcR (Awasaki et al., 2011). We found that astrocytes failed to transform into phagocytes in a background where *Myo^{RNAi}* was expressed in all glia but did so normally if we drove *Myo^{RNAi}* only in astrocytes (Fig. 8, A–I). Furthermore, we found that EcR-B1 staining was absent from astrocytes when *Myo^{RNAi}* was driven in all glia but normal when driven in astrocytes alone (Fig. 8, J–N). We interpret these data to mean that other glia (likely cortex and ensheathing glia) redundantly provide astrocytes with Myo to activate EcR expression, which then drives astrocyte transformation into phagocytes and, in turn, Beat-Va_M neuron local pruning. Since Myo knockdown in astrocytes alone did not block Beat-Va_M neuron local pruning, we speculate that other astrocyte-derived factors regulate the activation of Beat-Va_M neuron local pruning.

Beat-VaM neurite fragmentation and astrocyte transformation are tightly coupled

Neuronal immunoglobulin superfamily (IgSF) molecules have previously been shown to regulate neurite remodeling (Awasaki et al., 2011; Yu et al., 2013; Bornstein et al., 2021). We reasoned

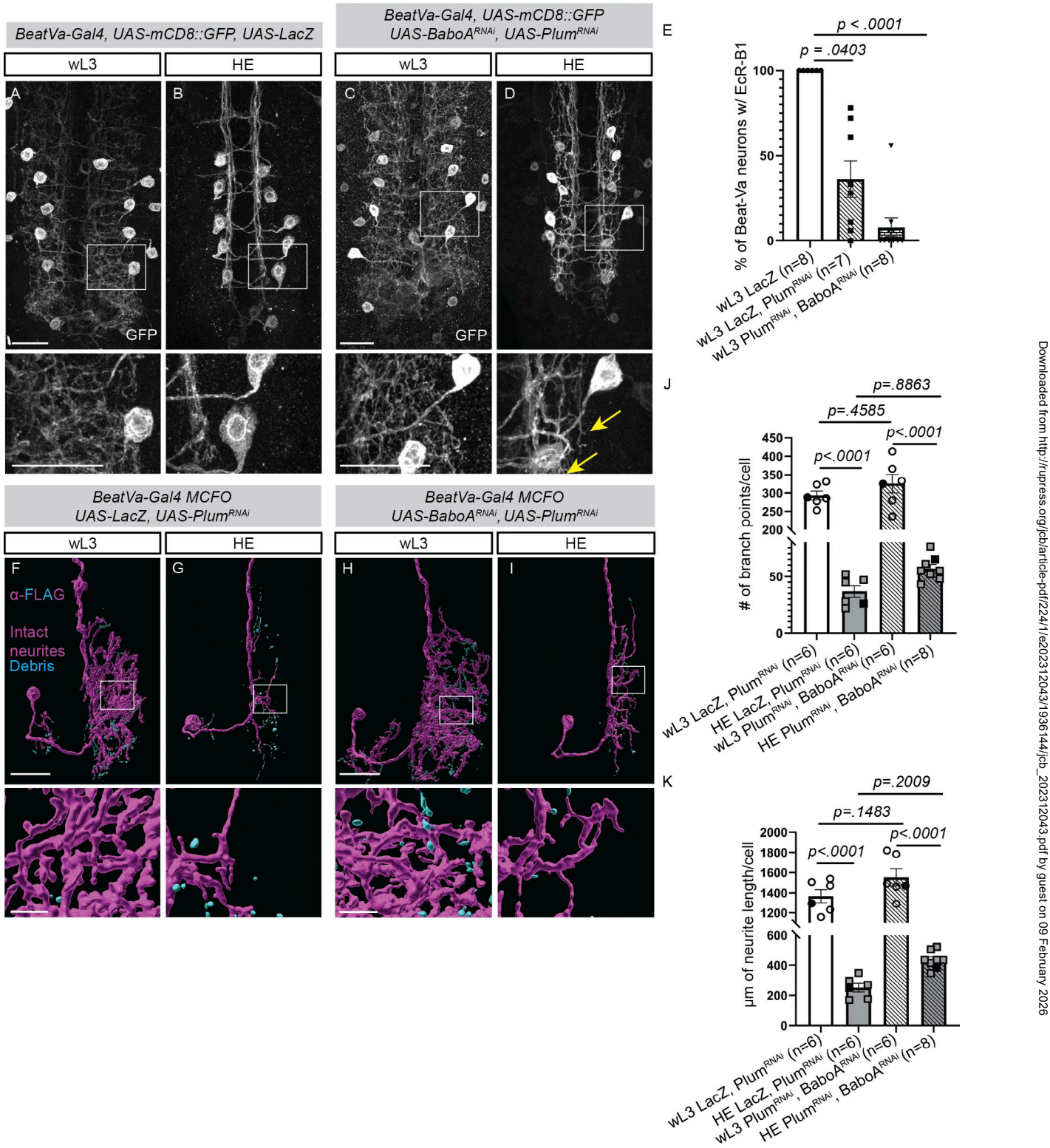

Figure 4. **Genetic depletion of EcR by targeting upstream regulators does not block Beat-Va$_M$ neuron remodeling. (A and B)** Beat-Va neurons labeled with mCD8::GFP at wL3 (A) or HE (B) while driving a *UAS-LacZ* as a control construct. Boxed area shown at higher magnification below. **(C and D)** Beat-Va neurons expressing *UAS-Plum^{RNAi}* and *UAS-BaboA^{RNAi}* to suppress EcR-B1 expression at wL3 (C) and HE (D). Remaining projections, yellow arrow. Scale bars are 20 µm. **(E)** Dual expression of *UAS-BaboA^{RNAi}* and *UAS-Plum^{RNAi}* resulted in substantial loss of EcR protein by antibody staining. One-way ANOVA, Kruskal-Wallis test for multiple comparisons. Each dot represents one animal. **(F and G)** Beat-Va$_M$ neurons driving *UAS-LacZ* and *UAS-Plum^{RNAi}* labeled using MCFO at wL3 (F) and HE (G). **(H and I)** Beat-Va$_M$ neurons driving *UAS-BaboA^{RNAi}* and *UAS-Plum^{RNAi}* labeled using MCFO at wL3 (H) and HE (I). Intact neurites, magenta; fragmented neurites, cyan. Boxed areas are shown in high magnification below the image. **(J and K)** Quantification of branch point number (J) and (K) neurite length for F–I. Comparison with two-way ANOVA and Sidak test for multiple comparisons. **(A–D)** Scale bars are 20 µm. **(F–I)** Surface renderings. Scale bars are 20 µm

in single cell images and 5 µm in the magnified view. **(J and K)** Each data point represents one cell. For wL3, LacZ Plum cells were imaged from four animals, for HE, LacZ Plum cells were imaged from five animals, for wL3 Plum, BaboA cells were imaged from four animals, and for HE Plum, BaboA cells were imaged from five animals. Colored data points correspond to the representative image shown in the figure. All error bars are SEM.

they, or other surface molecules, could encode the astrocyte cue or cues that instruct Beat-Va_M neurons to prune. We therefore screened 104 genes encoding for IgSF and other cell surface molecules using RNAi to knock each gene down in astrocytes (using *GMR25H07-Gal4*) and visualized Beat-Va_M neurites (using *Beat-LexA*, *LexAop-GFP*) along with astrocyte transformation into phagocytes (Fig. 9). With respect to pruning phenotypes, we found three phenotypes: (1) those that resulted in intact Beat-Va_M neurites at HE (*CG3164*, *Dpr2*, *DIP-ζ*, *Fipi*, *Sema2a*, and *Dpr16*) (Fig. 9, B–G); (2) those where Beat-Va_M neurites fragmented but neuronal debris was not cleared by HE (*CG15744*, *Babo*, *ImpL2*, *Kek5*, *Htl*, *Beat-IIIb*, and *Kek4*) (Fig. 9, H–N); and (3) those that gave an intermediate phenotype (*Fas3*, *Kek6*, *Vein*, *Wrapper*, *Dpr17*, *Dpr8*, *Dpr9*, and *Dscam2*) (Fig. 9, O–V). When we assayed

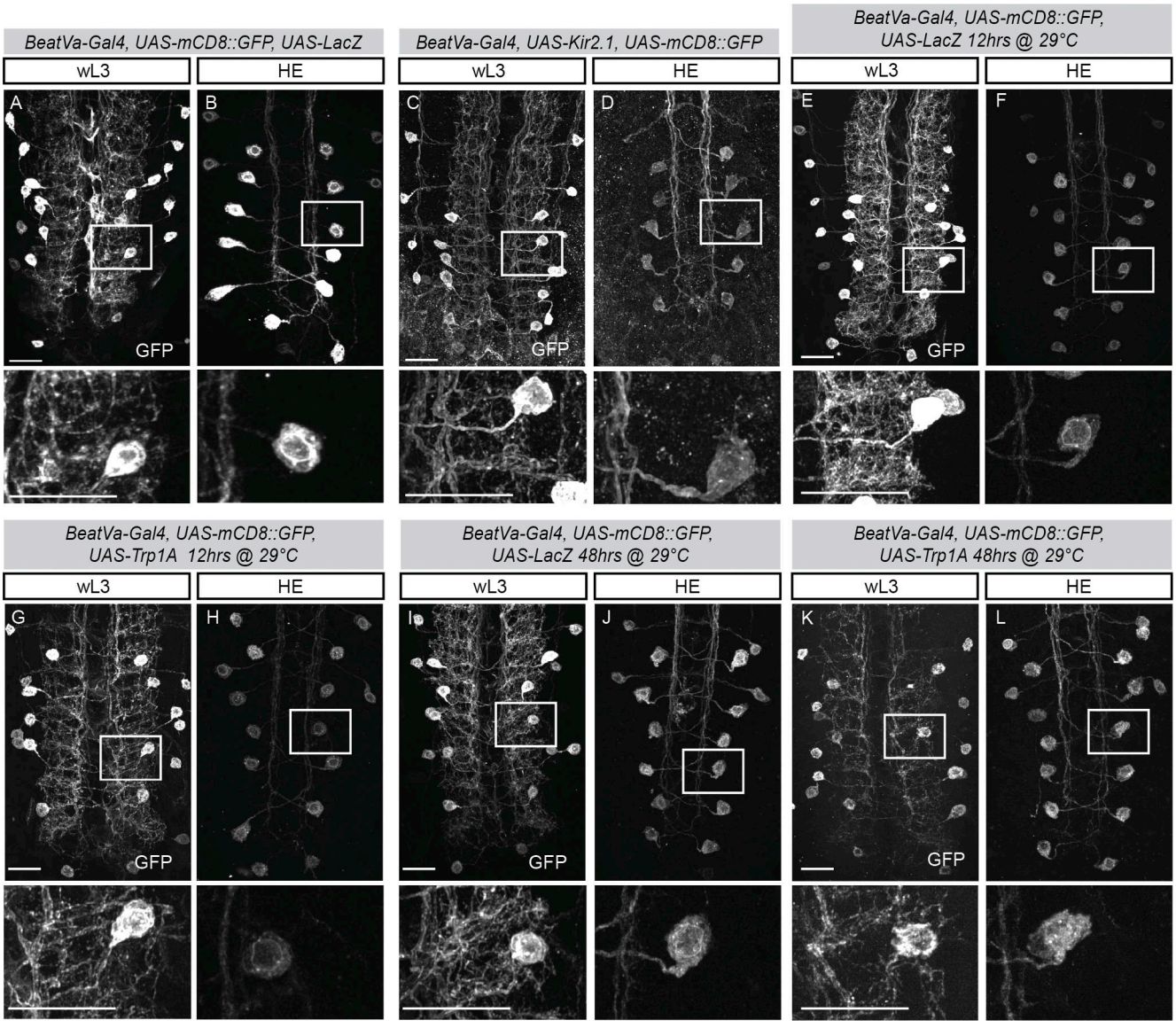

Figure 5. **Cell specific neuronal activity manipulation does not change Beat-Va_M pruning. (A and B)** Beat-Va neurons genetically labeled with mCD8::GFP and expressing *UAS-LacZ* at wL3 (A) and HE (B). **(C and D)** Beat-Va neurons genetically labeled with mCD8::GFP and constitutively expressing Kir2.1 under UAS control at wL3 (C) and HE (D). **(E and F)** Beat-Va neurons expressing LacZ under UAS control when at wL3 (E) and HE (F). The HE condition underwent metamorphosis at 29°C. **(G and H)** Beat-Va neurons expressing Trp1A, a temperature-sensitive cation channel, under UAS control at wL3 (G) and HE (H). The HE condition underwent metamorphosis at 29°C. **(I and J)** Beat-Va neurons expressing LacZ under UAS control at wL3 (I) and HE (J). All animals spent the 48 h prior to collection at 29°C. **(K and L)** Beat-Va neurons expressing Trp1A, under UAS control at wL3 (K) and HE (L). All animals spent the 48 h prior to collection at 29°C. All scale bars are 20 µm.

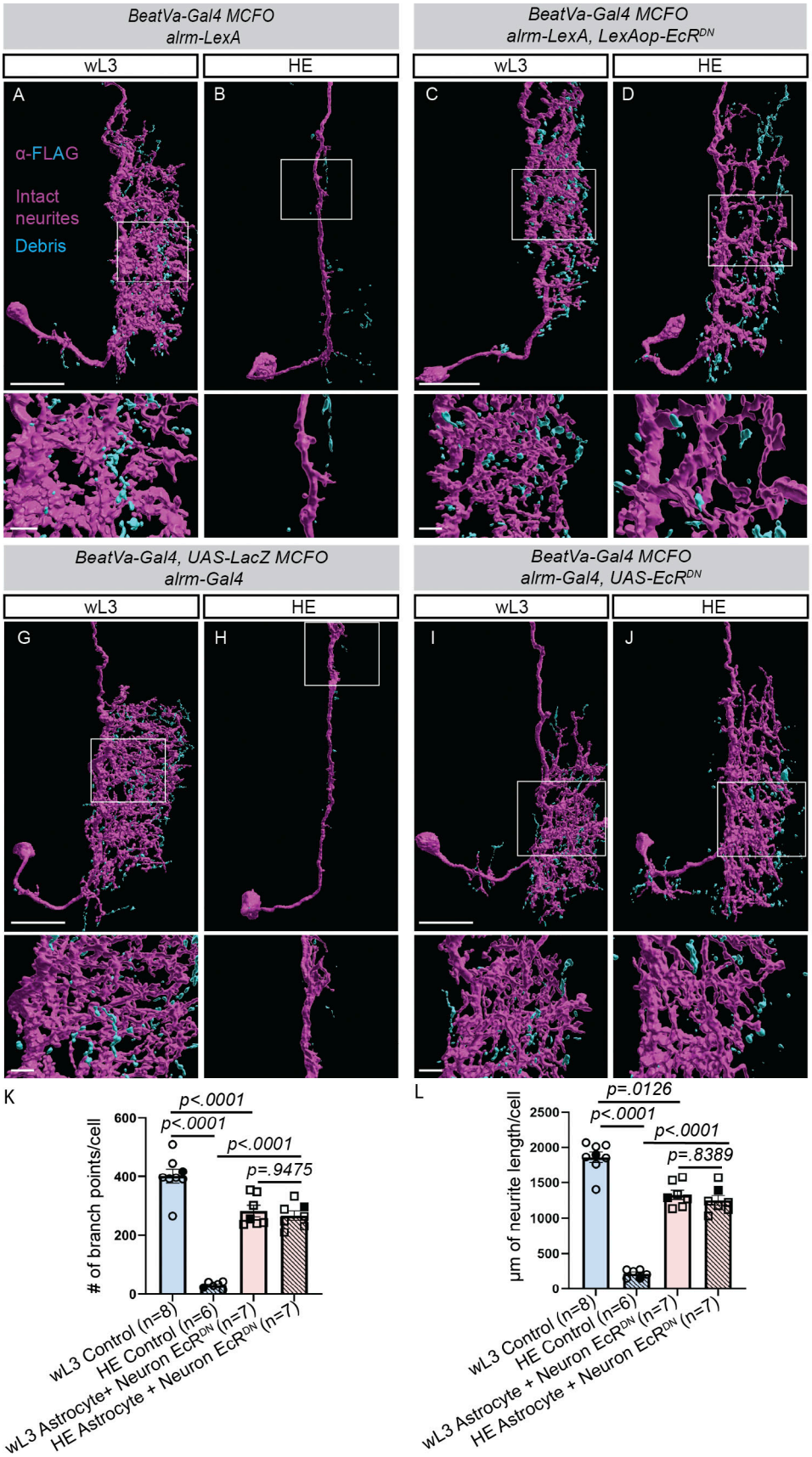

Figure 6. **Astrocyte-derived signals converge with intrinsic BeatVa$_M$ neuron EcR signaling to execute local pruning. (A and B)** Beat-Va$_M$ neurons labeled with MCFO in an *alrm-LexA* background (control) at wL3 (A) or HE (B). **(C and D)** *alrm-LexA, LexAOp-EcR^{DN}* background labeled with the MCFO technique

at wL3 (C) or HE (D). **(E and F)** Quantification of branch point number (E) or total neurite length (F) of A–D. **(G and H)** Beat-Va$_M$ neurons in an *alrm-Gal4* background (control) at wL3 (G) or HE (H). **(I and J)** Beat-Va$_M$ neurons in an *alrm-Gal4, UAS-EcR^{DN}* background at wL3 (I) or HE (J). **(K and L)** Quantification of branch point number (K) or total neurite length (L) of G–J. **(E and F)** Each data point represents one cell. wL3 control cells were imaged from six animals, HE control cells were imaged from six animals, wL3 astrocyte+neuron EcRDN cells were imaged from six animals, and HE astrocyte EcRDN cells were imaged from six animals. **(J and K)** Each data point represents one cell. wL3 control cells were imaged from six animals, HE control cells were imaged from five animals, wL3 astrocyte EcRDN cells were imaged from seven animals, HE astrocyte EcRDN cells were imaged from six animals. All comparisons are done with two-way ANOVA with the Sidak test for multiple comparisons. **(A–D and G–J)** Surface renderings. Intact neurites, magenta; fragmented neurites, cyan. Scale bars are 20 µm for whole neuron images and 5 µm for magnified images. Colored data points correspond to the representative image shown in the figure. All error bars are SEM.

astrocyte morphology at wL3, 4 h APF, and HE in RNAi backgrounds for *CG3164*, *Dpr2*, *DIP-ζ*, and *Fipi*, we found that astrocytes looked relatively healthy at wL3—as evaluated by their bushy processes infiltrating the neuropil—but at 4 h APF all astrocytes had failed to transform into phagocytes (assessed by a lack of large, clustered, vesicles) (Fig. 10, A–E″). In contrast, when we assayed astrocyte morphology in hits with defects in clearance of neuronal debris (*CG15744*, *Babo*, *ImpL2*, *Kek5*, *Htl*, *Beat-IIIb*, and *Kek4*), we found that astrocytes were highly vesiculated by 4 h APF, a hallmark of successful transformation into phagocytes (Fig. 10, F–H″). Collectively, these findings highlight a striking correlation between astrocyte phagocytic transformation and neurite fragmentation: if astrocytes did not transform into phagocytes, Beat-Va$_M$ neurons remained largely intact. These data reveal a tight correlation between astrocyte transformation into phagocytes and fragmentation of Beat-Va$_M$ neurons during local pruning and imply that astrocytes have a more active role in shaping this neural circuit than simply clearing pruned neuronal debris.

Discussion

A growing collection of mechanistic studies on neuronal remodeling suggests that a diversity of molecular pathways are deployed across the nervous system to accomplish remodeling in different contexts (Schafer et al., 2012; Neukomm and Freeman, 2014; Yaniv and Schuldiner, 2016; Boulanger and Dura, 2022). The relatively small number of neuronal populations in which remodeling has been studied, compared with the total number that likely exhibit remodeling across the CNS of complex metazoans, may have limited the depth of our knowledge about the diversity of signaling pathways that can drive cell death, and neurite or synaptic pruning. In this study, we identified the *BeatVa-Gal4*–expressing neurons and show they remodel using mechanisms not previously reported in other heavily studied CNS cell types: MB neurons (Lee et al., 2000; Yu et al., 2013; Lai et al., 2016) and ventral Corazonin neurons (Choi, 2006; Lee et al., 2013; Wang et al., 2019). Beat-Va$_M$ neurons exhibit EcR-independent, astrocyte-activated local neurite pruning, while Beat-Va$_L$ neurons die in a Hox gene-mediated, segmentally restricted pattern. The unique set of mechanisms that we found to underly Beat-Va neuron remodeling—among the first new neuronal subtypes whose remodeling we have characterized in detail—also supports the notion that a diversity of undiscovered remodeling mechanisms likely exist across the brain.

Beat-Va$_L$ neurons die in a caspase and steroid hormone-dependent fashion, similar to other neuronal cell types that undergo cell death at metamorphosis (Choi, 2006; Lee et al., 2013). However, we found that the Hox gene *Abd-B* controls the segment-specific patterns of Beat-Va$_L$ neuron cell death, with the three Abd-B–positive posterior Beat-Va$_L$ cells undergoing cell death, while the anterior two Abd-B–negative cells survive. Knocking down *Abd-B* in Beat-Va neurons blocked caspase activation and cell death in the posterior cells, while overexpressing *Abd-B* in Beat-Va neurons drove cell death in the two, normally surviving, anterior Beat-Va$_L$ cells. Notably, neither overexpression nor knockdown of *Abd-B* had any noticeable effect on Beat-Va$_M$ neuron local pruning. We propose that Abd-B confers positional identity that leads to cell death in the appropriate Beat-Va$_L$ cells.

Beat-Va$_M$ neurons undergo massive local neurite pruning during the first 12 h of metamorphosis, which we visualized with single-cell precision. Surprisingly, unlike all other neuronal cell types studied in *Drosophila*, we found that Beat-Va$_M$ neuron local pruning was not strongly suppressed by cell-autonomous blockade of EcR signaling. Rather, we found that blocking astrocyte developmental progression (into a phagocytic phenotype) using EcR^{DN} reduced Beat-Va$_M$ remodeling by ∼50%, and when combined with simultaneous blockade of EcR signaling in Beat-Va$_M$ neurons, local neurite pruning was almost entirely blocked. We proposed that extrinsic cues from phagocytic astrocytes and neuron-intrinsic EcR-mediated events converge to control Beat-Va$_M$ remodeling. Beat-Va$_M$ neurons should therefore provide an excellent system in which to genetically dissect astrocyte to neuron signaling pathways that promote local pruning.

Why a role for neuron-autonomous EcR signaling is more fully revealed when astrocytes are also blocked from transformation is an open question. A recent study showed that neuronal ecdysone signaling allows ddaC neurons to become competent for pruning by driving microtubule rearrangement, with subsequent physical force caused by tissue movement in the body wall during metamorphosis driving the severing and fragmentation of dendrites (Krämer et al., 2023). It is possible that neuronal ecdysone signaling may make Beat-Va$_M$ neurons competent for remodeling through similar mechanisms, but the execution of fragmentation requires a secondary mechanical event. Astrocytes could, for example, provide the physical force that severs small neurites during metamorphosis as they transform and become phagocytic. We certainly observed a tight correlation between astrocyte transformation and Beat-Va$_M$ neurite fragmentation. We noted that the fragmentation we observed when EcR signaling was blocked in Beat-Va$_M$ neurons occurred primarily in smaller-diameter Beat-Va$_M$ neurites.

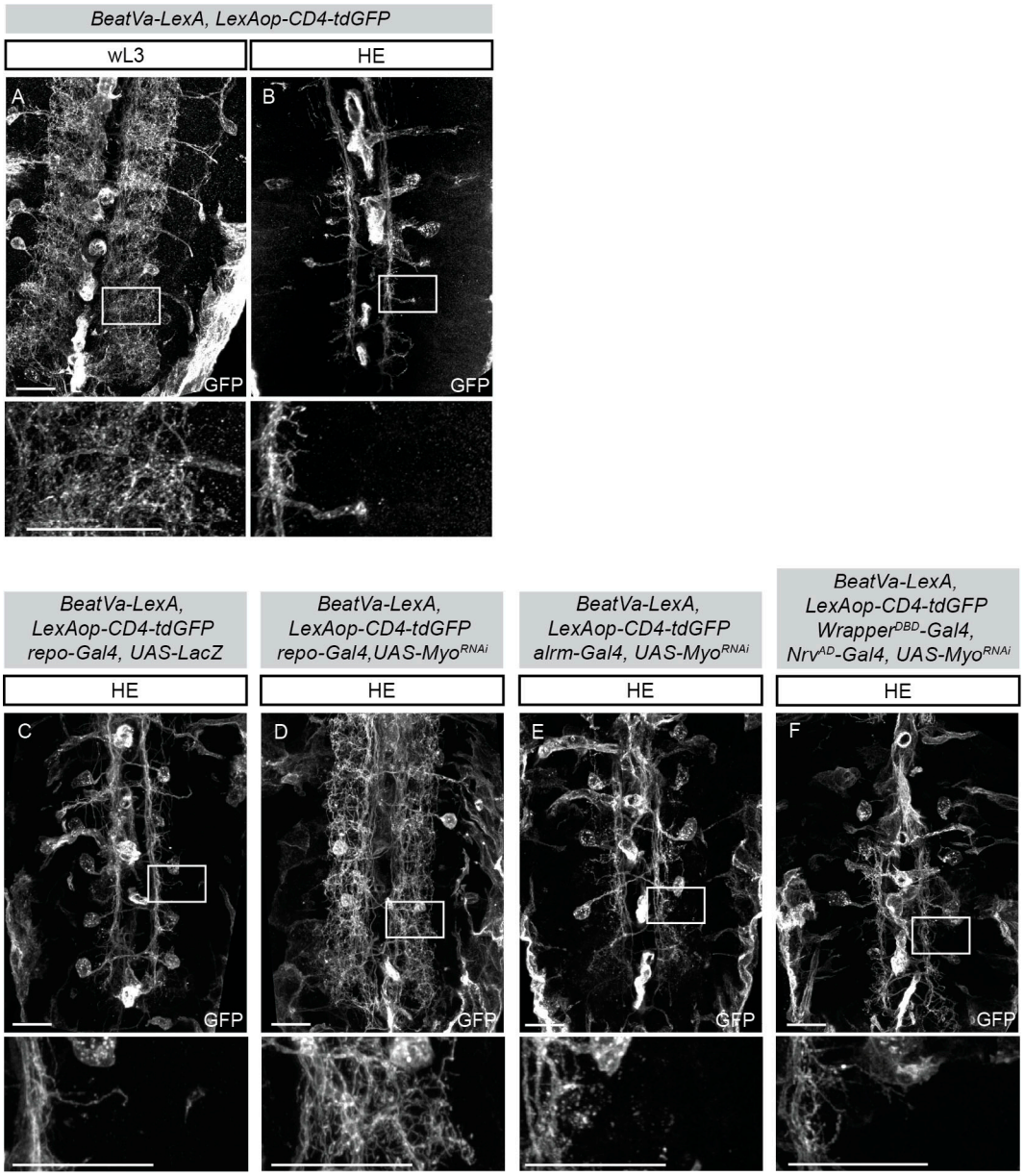

Figure 7. **Pan glial, but not astrocyte or cortex glia specific depletion of Myo, drives Beat-Va$_M$ neurite fragmentation. (A and B)** Beat-Va neurons labeled with a LexAop driven, CD4-tdGFP at wL3 (A) or HE (B). **(C)** Beat-Va$_M$ neurons at HE with *repo-Gal4* and *UAS-LacZ* (control) in the background. **(D)** Myo knocked down in all glia with *repo-Gal4*. **(E)** Myo knocked down only in astrocytes with *alrm-Gal4*. **(F)** Myo knocked down only in cortex glia with *wrapper^{DBD}-Gal4, Nrv-Gal4AD*. Eight animals were checked for each time point and genotype shown in this figure, and the morphology and phenotypes shown are representative of what was observed. All scale bars are 20 µm.

Perhaps the architectural integrity of large versus small diameter of a neuronal process makes fine neurite processes more susceptible to remodeling, as larger processes are more likely to be microtubule rich while smaller processes are more likely actin-based.

Do astrocytes release molecular cues onto neurites as they transform into phagocytes that promote the progression of neurite remodeling? The glial-secreted TGFβ ligand Myo is known to activate the expression of EcR in neurons, thereby establishing their competence to prune in response to ecdysone (Awasaki et al., 2011; Yu et al., 2013; Hakim et al., 2014; Wang et al., 2019). We found that depletion of Myo from astrocytes did not block Beat-Va$_M$ neuron local pruning nor astrocyte transformation but pan-glial Myo depletion led to decreased EcR expression in astrocytes and a failure of astrocytes to transform. We proposed that Myo released redundantly by the cortex or ensheathing glia promotes EcR expression in astrocytes during early metamorphosis, which can then activate the phagocytic (or remodeling) program in astrocytes. To begin to explore the nature of astrocytic cues that might drive Beat-Va$_M$ remodeling, we performed a targeted forward genetic screen for astrocyte molecules required for Beat-Va$_M$ pruning. Although our screen explored roles for only transmembrane IgSF molecules on astrocytes, the

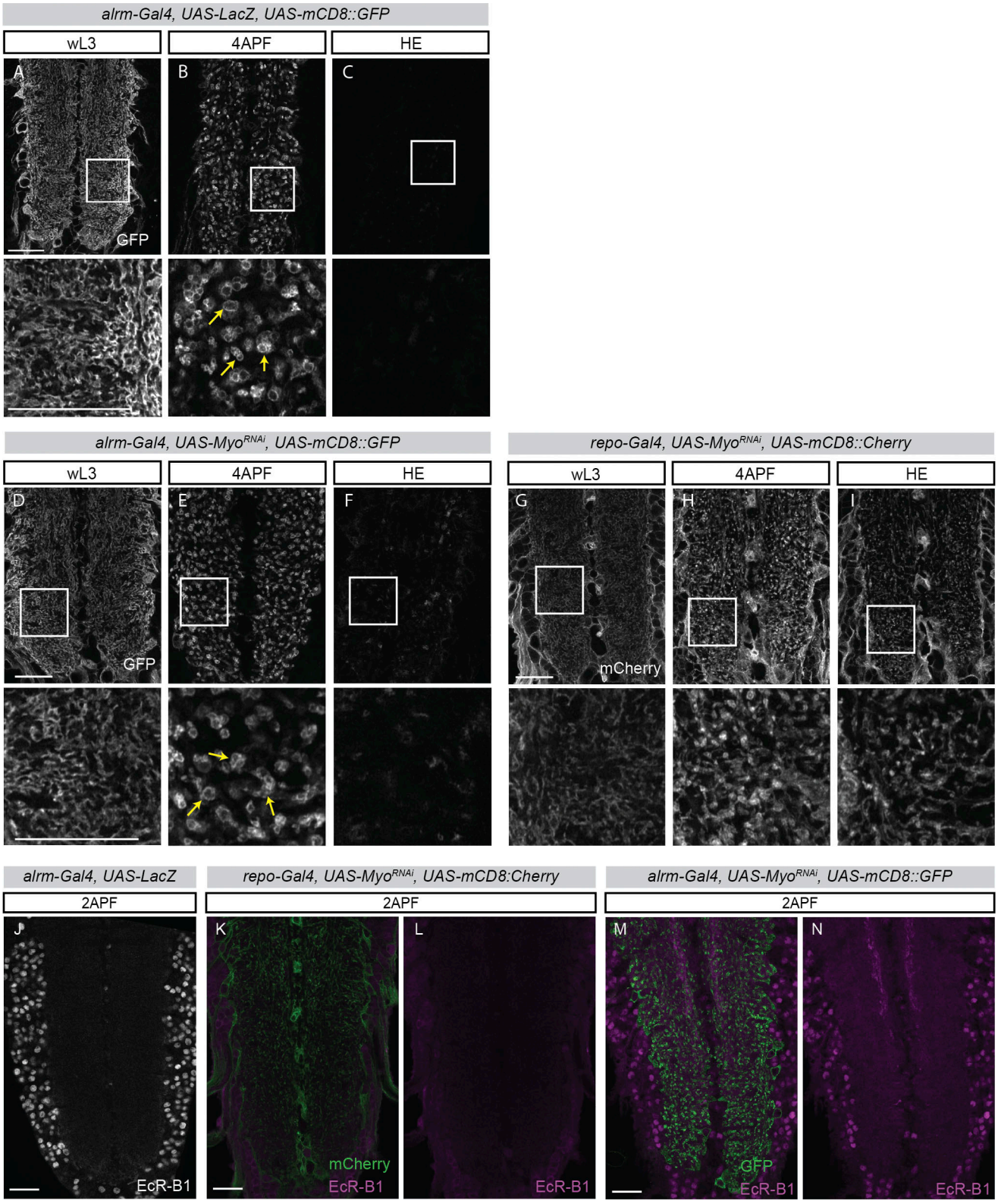

Figure 8. **Pan-glial Myo induces phagocytic astrocyte transformation. (A–C)** Astrocytes labeled with a membrane targeted GFP (*UAS-mCD8::GFP*) at wL3 (A), 4APF (B), and HE (C), showing the typical tranformation from circuit support cells with "wispy" processes at wL3 to phagocytic cells with vesicles (yellow arrows) at 4 h APF, to largely absent from the neuropil at HE. **(D–F)** Myo knocked down only in astrocytes with *alrm-Gal4*. Astrocytes look morphologically normal at wL3 (D), continue to transform into phagocytes by 4 h APF (E) with vesicles (yellow arrows), and then largely disappear from the neuropil by HE (F). **(G–I)** Visualization of astrocytes using *a UAS-mCD8::Cherry* when Myo is knocked down in all glia. Astrocytes look morphologically normal at wL3 (G) but fail to transform into phagocytes with vesicles at 4 h APF (H) and continue to persist, albeit without phagocytic vesicles, to HE (I). **(J)** EcR-B1 staining in a *alrm-Gal4, UAS-LacZ* (control) animal. **(K and L)** Expression of *UAS-Myo^{RNAi}* in all glia, EcR-B1 staining (magenta). Astrocyte membranes, green. **(M and N)** Expression of *UAS-Myo^{RNAi}* in astrocytes, EcR-B1 staining, magenta. Astrocyte membranes, green. Six to eight animals were checked for each time point and genotype shown in this figure, and the morphology and phenotypes shown are representative of what was observed. All scale bars are 20 µm.

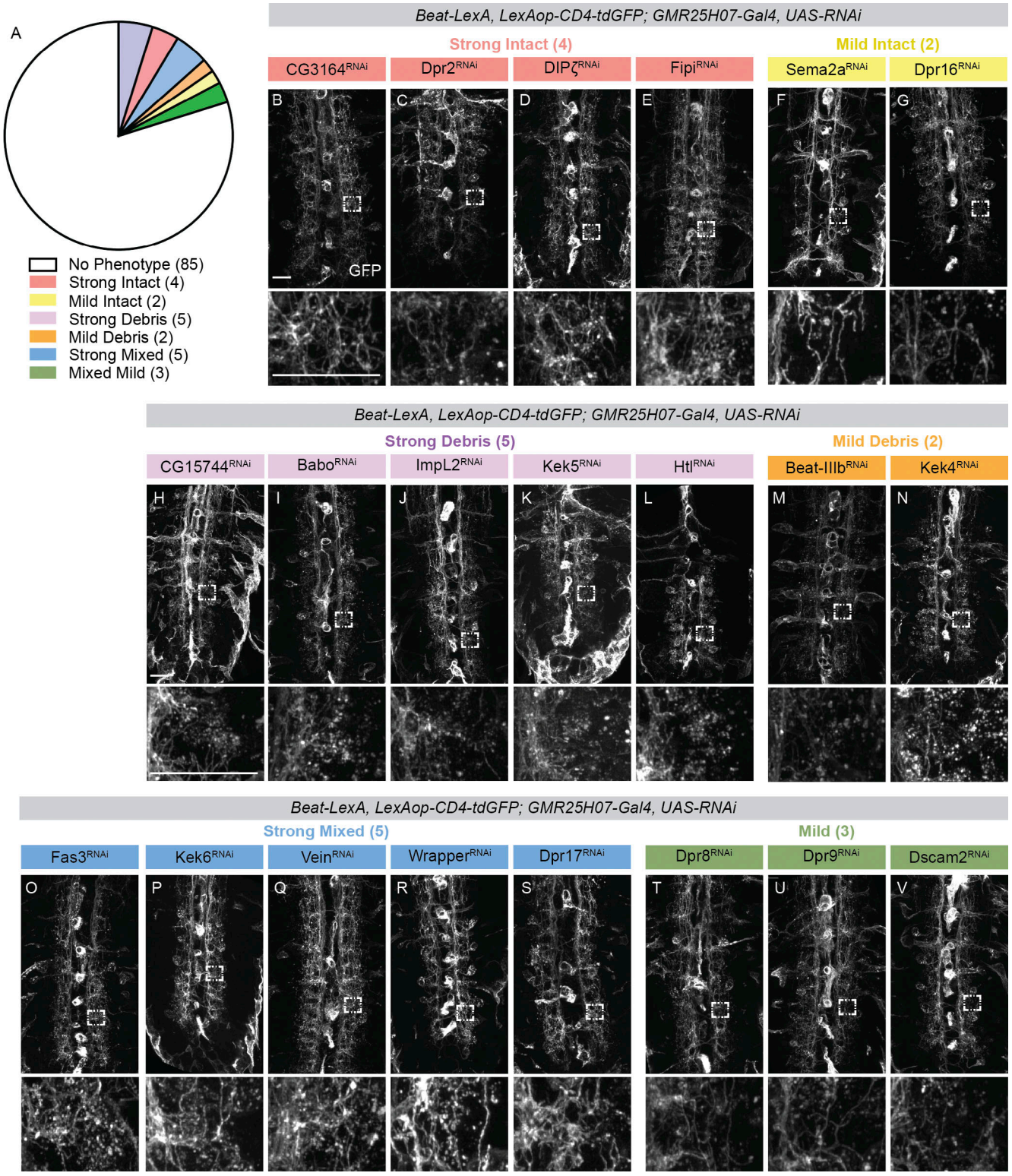

Figure 9. **Small scale genetic screen identifies astrocytic cues that drive Beat-Va$_M$ remodeling. (A)** Pie chart summarizing the results of the screen, indicating the number of lines per phenotypic category. Astrocyte knockdown of candidate molecules was achieved by UAS-driven RNAi's, and Beat-Va neurons were visualized with *Beat-LexA*–driven *CD4-tdGFP*. **(B–V)** Show Beat-VaM neurons, grouped by phenotype and color-coded to match the pie chart in A, with the gene which the RNAi targeted indicated above the corresponding image. Scale bar is 20 µm. Five animals were examined per condition, and phenotypes shown are representative of what was observed.

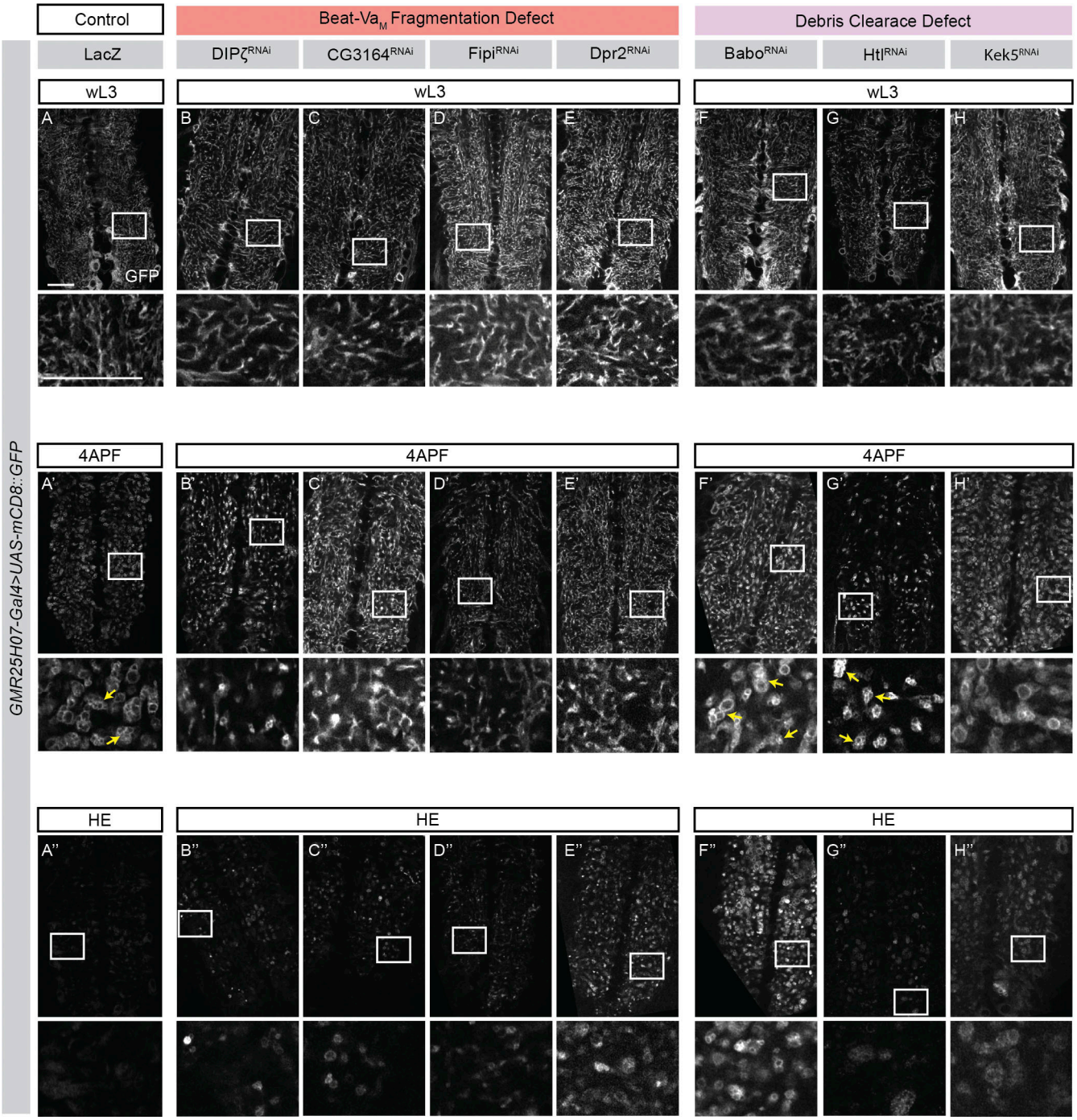

Figure 10. **Astrocyte transformation correlates strongly with Beat-VaM neurite fragmentation. (A–A″)** Astrocytes expressing a *UAS-LacZ* (control) labeled with a membrane-targeted GFP (*UAS-mCD8::GFP*) at wL3 (A), 4 h APF (A′), and HE (A″). **(B–E″)** Astrocytes expressing *UAS-DIPζ^{RNAi}* (B–B″), *UAS-CG3164^{RNAi}* (C–C″), *UAS-Fipi^{RNAi}* (D–D″), *UAS-Dpr2^{RNAi}* (E–E″) labeled with a membrane-targeted GFP (*UAS-mCD8::GFP*) at wL3, 4APF, and HE. All manipulations show a stark lack of transformation of astrocytes into phagocytes at 4 h APF, as evidenced by lack of vesicles (B′–E′). **(F–H″)** Astrocytes expressing *UAS-Babo^{RNAi}* (F–F″), *UAS-Htl^{RNAi}* (G–G″), *UAS-Kek5^{RNAi}* (H–H″). Knockdown of these genes do not noticeably disrupt the transformation of astrocytes into phagocytes, as all 4 h APF animals (F′–H′) still exhibit vesicle formation. Scale bars are 20 µm. Yellow arrows denote correctly formed phagocytic veiscles.

overall results were informative. We found a tight correlation between astrocyte transformation and fragmentation of Beat-Va$_M$ neurites—Beat-Va$_M$ neurites only fragmented if astrocytes transformed into phagocytes. If these two processes were genetically separable, we might have expected to find a genetic manipulation where astrocytes transformed into phagocytes while neurites remained intact. Perhaps perturbation of other transmembrane or secreted molecules in the future will result in such a phenotype? Alternatively, it is possible that similar to peripheral dendrites, astrocyte phagocytic transformation enables them to physically break down CNS neurites as a normal part of local pruning.

Materials and methods

Resource table

See Table S4 for information on reagents used, including *Drosophila* lines, antibodies, and software.

Drosophila genetics

Drosophila melanogaster was reared using standard laboratory conditions. All experiments were conducted at 25°C unless otherwise explicitly noted. A complete list of all fly strains used in this study can be found in the key resource table.

Immunohistochemistry

Dissection and immunostaining of larval and pupal fly brains were performed according to an adapted FlyLight protocol (Jenett et al., 2012). Larval brains were dissected in cold PBST (phosphate buffered saline; Invitrogen) with 0.1% Triton X-100 and fixed at 4% formaldehyde (Electron Microscopy Sciences) for 20 min at room temperature. Fixed brains were washed three times with PBS while nutating at room temperature for 10–15 min per wash. Primary and secondary antibodies were diluted in PBST (0.1% Triton X-100) and incubated with samples at 4°C for 24–48 h. Washes after antibody incubations were performed at room temperature with PBS for 3 × 15 min. Samples were mounted in VECTASHIELD antifade mounting medium (Vector Laboratories) and stored at 4°C until imaging.

Image analysis and processing

Imaging was performed using a Zeiss LSM 880 with Airyscan. Confocal z-stacks were acquired using the optimal z-interval and 0.05–0.09 µm/pixel resolution with a 40×/1.3 Plan-Apochromat oil objective. Images were-Airyscan processed with Zeiss' ZEN Black software, image tiles stitched with a 6–8% overlap when necessary, and converted into IMARIS format for 3D analysis. 3D rendering was performed with IMARIS; and single image or z-stack projections were analyzed in ImageJ. All imaging was done at 25°C.

Image analysis

To quantify individual neuronal morphologies, we used the Surface module in IMARIS 10 (Bitplane) with the Filament module. The module was trained on example images through iterative machine learning and then the algorithm was applied to all images. The first 100 µm of each neuron after it crossed the midline was analyzed for both total filament length and number of branch points. To determine if a neurite was intact or fragmented, individual filaments were then examined with the micrograph overlayed on the rendering. If a break in a neurite was observed (an area of any length without neurite labeling), the filament was discarded.

Data analysis and statistics

All statistical analyses were carried out using GraphPad Prism 9; statistical details, P values, and sample sizes are indicated in the figure legends. Any comparison between two parametric data sets that only had one independent variable was conducted with a Student's *t* test. Any comparison between >2 parametric data sets that only had one independent variable was conducted with a one-way ANOVA with the Sidak test for multiple comparisons. Any comparison between >2 non-parametric data sets that only had one independent variable was conducted with a one-way ANOVA with the Kruskal-Wallis test for multiple comparisons. Any comparison between >2 parametric data sets that had two independent variables was conducted with a two-way ANOVA with the Sidak test for multiple comparisons. Parametric data distribution was assumed to be normal but this was not formally tested. For all graphs accompanied by imaging data, the data point that corresponds to the image shown is colored.

Generating *BeatVa-LexA* stock

BeatVa-LexA lines were made with Gateway cloning. The 3,471 base pair enhancer region was cloned with primer sequences provided on the Janelia Flylight page. They were cloned into the *pBPnlsLexAGADflUw* vector (#26232; Addgene) and verified through Sanger sequencing (Genewiz). Injections were site directed using the $y^1\ w^{67c23}$; *P[CaryP attP2]* line (BL8622), $y^1\ w^{67c23}$ *P[CaryP attP18]* (BL 32107) line and $y^1\ w^{67c23}$; *P[CaryP attP40]* line. The attp18 insertion was used in all the above experiments. The line was verified by comparing GFP expression generation from the *Beat-LexA* line driving a *LexAop-GFP* to a *BeatVa-Gal4* line driving a *UAS-mCD8::cherry*.

Generating *LexAop-EcR^{DN}* stock

The *LexAop-EcR^{DN}* construct was created by amplifying DNA from flies containing *UAS-EcR.B1DC655.W650A* (Bloomington *Drosophila* Stock Center). The amplification was carried out using the EcR^{DN} Kozak *AgeI* F primer (5′-CCCCCAACCGGTCAAAACATGAAGCGGCGCTGGTCGAACA-3′) and EcR$^{DN\text{-}W650A}$ *XbaI* R primer (5′-CCCAATCTAGACTAGATGGCATGAACGTCGGCGA-3′). The resulting PCR product was digested with AgeI and XbaI (NEB) and then ligated into the *pattB-13xLexAop2EGFP* plasmid (Coutinho-Budd et al., 2017), with GFP removed via *AgeI* and *XbaI* digestion. The final construct, *pattB-13xLexAop2-EcR^{W650A}*, was generated through ligation using T4 ligase (NEB), and the transformation was carried out in *DH5α* cells (Zymo). The construct's sequence was verified through Sanger sequencing (Genewiz), and it was utilized for attp154 landing site-specific integration on the second chromosome (Bestgene).

Online supplemental material

Fig. S1 shows how we established the segmental characterization of Beat-Va neurons. Fig. S2 shows the segmental breakdown of Beat-Va$_L$ and Beat-Va$_M$ caspase activation. Fig. S3 contains supporting data about Abd-B and EcR-B1 localization in wildtype and knockdown conditions. Fig. S4 shows astrocyte transformation in wildtype conditions and when EcR signaling is blocked specifically in astrocytes; additionally, it shows micrographs of Beat-Va$_M$ neurons in these conditions. Fig. S5 verifies the overlap between the *BeatVa-Gal4* line and the *BeatVa-LexA* line. Table S1 is the in vivo evaluation of *Drosophila* lines from the Janelia Flylight collection at wL3, while Table S2 evaluates a subset of these lines at multiple time points. Table S3 describes the phenotypes from our targeted screen to drive astrocyte-mediated Beat-Va$_M$ neuronal remodeling. Table S4 lists our reagents, including *Drosophila* lines, antibodies, software and

algorithms, and cloning reagents. The source and RRID identifier for each reagent are also listed.

Data availability

Raw data underlying this study is available from the corresponding author upon request.

Acknowledgments

We would like to acknowledge all members of the Freeman lab for thoughtful discussions and suggestions throughout this project. We acknowledge the fly community for the generous sharing of reagents.

This study was supported by National Science Foundation Graduate Research Fellowship Program Fellowship DGE-1448072 (to K.S. Lehmann), Damon Runyon Fellowship DRG 2329-18 (to Y. Kang), National Institutes of Health (NIH) grant K99 NS126642-01 (to Y. Kang), and NIH/National Institute of Neurological Disorders and Stroke RO1s R37NS053538 and R01NS124146 (to M.R. Freeman).

Author contributions: K.S. Lehmann: Conceptualization, Data curation, Formal analysis, Funding acquisition, Investigation, Methodology, Project administration, Validation, Visualization, Writing - original draft, Writing - review & editing, M.T. Hupp: Data curation, Investigation, Visualization, Writing - review & editing, L. Abalde-Atristain: Data curation, Formal analysis, Investigation, Validation, Writing - review & editing, A. Jefferson: Data curation, Investigation, Validation, Writing - review & editing, Y.-C. Cheng: Resources, A.E. Sheehan: Investigation, Resources, Y. Kang: Conceptualization, Data curation, Investigation, Methodology, Project administration, Supervision, Validation, Visualization, Writing - review & editing, M.R. Freeman: Conceptualization, Funding acquisition, Methodology, Project administration, Resources, Supervision, Writing - original draft, Writing - review & editing.

Disclosures: The authors declare no competing interests exist.

Submitted: 7 December 2023
Revised: 1 July 2024
Accepted: 5 September 2024

References

Atz, M.E., B. Rollins, and M.P. Vawter. 2007. NCAM1 association study of bipolar disorder and schizophrenia: Polymorphisms and alternatively spliced isoforms lead to similarities and differences. *Psychiatr. Genet.* 17: 55–67. https://doi.org/10.1097/YPG.0b013e328012d850

Awasaki, T., Y. Huang, M.B. O'Connor, and T. Lee. 2011. Glia instruct developmental neuronal remodeling through TGF-β signaling. *Nat. Neurosci.* 14:821–823. https://doi.org/10.1038/nn.2833

Baines, R.A., J.P. Uhler, A. Thompson, S.T. Sweeney, and M. Bate. 2001. Altered electrical properties in Drosophila neurons developing without synaptic transmission. *J. Neurosci.* 21:1523–1531. https://doi.org/10.1523/JNEUROSCI.21-05-01523.2001

Bakshi, A., R. Sipani, N. Ghosh, and R. Joshi. 2020. Sequential activation of Notch and Grainyhead gives apoptotic competence to Abdominal-B expressing larval neuroblasts in Drosophila Central nervous system. *PLoS Genet.* 16:e1008976. https://doi.org/10.1371/journal.pgen.1008976

Bornstein, B., H. Meltzer, R. Adler, I. Alyagor, V. Berkun, G. Cummings, F. Reh, H. Keren-Shaul, E. David, T. Riemensperger, and O. Schuldiner. 2021. Transneuronal Dpr12/DIP-δ interactions facilitate compartmentalized dopaminergic innervation of Drosophila mushroom body axons. *EMBO J.* 40:e105763. https://doi.org/10.15252/embj.2020105763

Boulanger, A., and J.-M. Dura. 2022. Neuron-glia crosstalk in neuronal remodeling and degeneration: Neuronal signals inducing glial cell phagocytic transformation in Drosophila. *BioEssays.* 44:e2100254. https://doi.org/10.1002/bies.202100254

Boulanger, A., C. Thinat, S. Züchner, L.G. Fradkin, H. Lortat-Jacob, and J.-M. Dura. 2021. Axonal chemokine-like Orion induces astrocyte infiltration and engulfment during mushroom body neuronal remodeling. *Nat. Commun.* 12:1849. https://doi.org/10.1038/s41467-021-22054-x

Cherbas, L., X. Hu, I. Zhimulev, E. Belyaeva, and P. Cherbas. 2003. EcR isoforms in Drosophila: Testing tissue-specific requirements by targeted blockade and rescue. *Development*. 130:271–284. https://doi.org/10.1242/dev.00205

Choi, Y.J. 2006. Programmed cell death mechanisms of identifiable peptidergic neurons in Drosophila melanogaster. *Development*. 133: 2223–2232. https://doi.org/10.1242/dev.02376

Chung, W.-S., L. Clarke, G. Wang, B. Stafford, A. Sher, C. Chakraborty, J. Joung, L. Foo, A. Thompson, C. Chen, et al. 2013. Astrocytes mediate synapse elimination through MEGF10 and MERTK pathways. *Nature*. 504:394–400. https://doi.org/10.1038/nature12776

Clarembaux-Badell, L., P. Baladrón-de-Juan, H. Gabilondo, I. Rubio-Ferrera, I. Millán, C. Estella, F.S. Valverde-Ortega, I.M. Cobeta, S. Thor, and J. Benito-Sipos. 2022. Dachshund acts with Abdominal-B to trigger programmed cell death in the Drosophila central nervous system at the frontiers of Abd-B expression. *Dev. Neurobiol.* 82:495–504. https://doi.org/10.1002/dneu.22894

Clem, R.J., M. Fechheimer, and L.K. Miller. 1991. Prevention of apoptosis by a baculovirus gene during infection of insect cells. *Science*. 254:1388–1390. https://doi.org/10.1126/science.1962198

Coutinho-Budd, J.C., A.E. Sheehan, and M.R. Freeman. 2017. The secreted neurotrophin Spätzle 3 promotes glial morphogenesis and supports neuronal survival and function. *Genes Dev.* 31:2023–2038. https://doi.org/10.1101/gad.305888.117

Delorenzi, M., and M. Bienz. 1990. Expression of Abdominal-B homeoproteins in Drosophila embryos. *Development*. 108:323–329. https://doi.org/10.1242/dev.108.2.323

Denton, D., B. Shravage, R. Simin, E.H. Baehrecke, and S. Kumar. 2010. Larval midgut destruction in Drosophila: Not dependent on caspases but suppressed by the loss of autophagy. *Autophagy*. 6:163–165. https://doi.org/10.4161/auto.6.1.10601

Doherty, J., M.A. Logan, O.E. Taşdemir, and M.R. Freeman. 2009. Ensheathing glia function as phagocytes in the adult Drosophila brain. *J. Neurosci.* 29:4768–4781. https://doi.org/10.1523/JNEUROSCI.5951-08.2009

Feinberg, I. 1982. Schizophrenia: Caused by a fault in programmed synaptic elimination during adolescence? *J. Psychiatr. Res.* 17:319–334. https://doi.org/10.1016/0022-3956(82)90038-3

Freeman, M.R., J. Delrow, J. Kim, E. Johnson, and C.Q. Doe. 2003. Unwrapping glial biology: Gcm target genes regulating glial development, diversification, and function. *Neuron*. 38:567–580. https://doi.org/10.1016/S0896-6273(03)00289-7

Gunner, G., L. Cheadle, K.M. Johnson, P. Ayata, A. Badimon, E. Mondo, M.A. Nagy, L. Liu, S.M. Bemiller, K.W. Kim, et al. 2019. Sensory lesioning induces microglial synapse elimination via ADAM10 and fractalkine signaling. *Nat. Neurosci.* 22:1075–1088. https://doi.org/10.1038/s41593-019-0419-y

Hakim, Y., S.P. Yaniv, and O. Schuldiner. 2014. Astrocytes play a key role in Drosophila mushroom body axon pruning. *PLoS One*. 9:e86178. https://doi.org/10.1371/journal.pone.0086178

Hamada, F.N., M. Rosenzweig, K. Kang, S.R. Pulver, A. Ghezzi, T.J. Jegla, and P.A. Garrity. 2008. An internal thermal sensor controlling temperature preference in Drosophila. *Nature*. 454:217–220. https://doi.org/10.1038/nature07001

Hara, Y., K. Hirai, Y. Togane, H. Akagawa, K. Iwabuchi, and H. Tsujimura. 2013. Ecdysone-dependent and ecdysone-independent programmed cell death in the developing optic lobe of Drosophila. *Dev. Biol.* 374:127–141. https://doi.org/10.1016/j.ydbio.2012.11.002

Heisenberg, M. 1998. What do the mushroom bodies do for the insect brain? An introduction. *Learn. Mem.* 5:1–10. https://doi.org/10.1101/lm.5.1.1

Hoeppner, D.J., M.O. Hengartner, and R. Schnabel. 2001. Engulfment genes cooperate with ced-3 to promote cell death in Caenorhabditis elegans. *Nature*. 412:202–206. https://doi.org/10.1038/35084103

Hoopfer, E.D., A. Penton, R.J. Watts, and L. Luo. 2008. Genomic analysis of Drosophila neuronal remodeling: A role for the RNA-binding protein

boule as a negative regulator of axon pruning. *J. Neurosci.* 28:6092–6103. https://doi.org/10.1523/JNEUROSCI.0677-08.2008

Hutchins, J.B., and S.W. Barger. 1998. Why neurons die: Cell death in the nervous system. *Anat. Rec.* 253:79–90. https://doi.org/10.1002/(SICI)1097-0185(199806)253:3<79::AID-AR4>3.0.CO;2-9

Iram, T., Z. Ramirez-Ortiz, M.H. Byrne, U.A. Coleman, N.D. Kingery, T.K. Means, D. Frenkel, and J. El Khoury. 2016. Megf10 is a receptor for C1Q that mediates clearance of apoptotic cells by astrocytes. *J. Neurosci.* 36:5185–5192. https://doi.org/10.1523/JNEUROSCI.3850-15.2016

Ishizuka, K., Y. Fujita, T. Kawabata, H. Kimura, Y. Iwayama, T. Inada, Y. Okahisa, J. Egawa, M. Usami, I. Kushima, et al. 2017. Rare genetic variants in CX3CR1 and their contribution to the increased risk of schizophrenia and autism spectrum disorders. *Transl. Psychiatry*. 7:e1184. https://doi.org/10.1038/tp.2017.173

Jenett, A., G.M. Rubin, T.T. Ngo, D. Shepherd, C. Murphy, H. Dionne, B.D. Pfeiffer, A. Cavallaro, D. Hall, J. Jeter, et al. 2012. A GAL4-driver line resource for Drosophila neurobiology. *Cell Rep.* 2:991–1001. https://doi.org/10.1016/j.celrep.2012.09.011

Ji, H., B. Wang, Y. Shen, D. Labib, J. Lei, X. Chen, M. Sapar, A. Boulanger, J.M. Dura, and C. Han. 2023. The Drosophila chemokine-like Orion bridges phosphatidylserine and Draper in phagocytosis of neurons. *Proc. Natl. Acad. Sci. USA*. 120:e2303392120. https://doi.org/10.1073/pnas.2303392120

Jiakun, C., S. Tobias, K. Yunsik, S. Amy, P. Cameron, R.M. Kelly, and R.F. Marc. 2022. The Tre1/S1pr1 phospholipid-binding G protein-coupled receptor signaling pathway is required for astrocyte morphogenesis. *bioRxiv*. https://doi.org/10.1101/2022.09.15.508188 (Preprint posted September 17, 2022).

Karpova, N., Y. Bobinnec, S. Fouix, P. Huitorel, and A. Debec. 2006. Jupiter, a new Drosophila protein associated with microtubules. *Cell Motil. Cytoskeleton*. 63:301–312. https://doi.org/10.1002/cm.20124

Kirilly, D., Y. Gu, Y. Huang, Z. Wu, A. Bashirullah, B.C. Low, A.L. Kolodkin, H. Wang, and F. Yu. 2009. A genetic pathway composed of Sox14 and Mical governs severing of dendrites during pruning. *Nat. Neurosci.* 12:1497–1505. https://doi.org/10.1038/nn.2415

Koelle, M.R., W.S. Talbot, W.A. Segraves, M.T. Bender, P. Cherbas, and D.S. Hogness. 1991. The Drosophila EcR gene encodes an ecdysone receptor, a new member of the steroid receptor superfamily. *Cell*. 67:59–77. https://doi.org/10.1016/0092-8674(91)90572-G

Krämer, R., N. Wolterhoff, M. Galic, and S. Rumpf. 2023. Developmental pruning of sensory neurites by mechanical tearing in Drosophila. *J. Cell Biol.* 222:e202205004. https://doi.org/10.1083/jcb.202205004

Kuo, C.T., L.Y. Jan, and Y.N. Jan. 2005. Dendrite-specific remodeling of Drosophila sensory neurons requires matrix metalloproteases, ubiquitin-proteasome, and ecdysone signaling. *Proc. Natl. Acad. Sci. USA*. 102:15230–15235. https://doi.org/10.1073/pnas.0507393102

Lai, Y.-W., S.-Y. Chu, J.-Y. Wei, C.-Y. Cheng, J.-C. Li, P.-L. Chen, C.-H. Chen, and H.-H. Yu. 2016. Drosophila microRNA-34 impairs axon pruning of mushroom body γ neurons by downregulating the expression of ecdysone receptor. *Sci. Rep.* 6:39141. https://doi.org/10.1038/srep39141

Lee, T., and L. Luo. 1999. Mosaic analysis with a repressible cell marker for studies of gene function in neuronal morphogenesis. *Neuron*. 22:451–461. https://doi.org/10.1016/S0896-6273(00)80701-1

Lee, T., A. Lee, and L. Luo. 1999. Development of the Drosophila mushroom bodies: Sequential generation of three distinct types of neurons from a neuroblast. *Development*. 126:4065–4076. https://doi.org/10.1242/dev.126.18.4065

Lee, T., S. Marticke, C. Sung, S. Robinow, and L. Luo. 2000. Cell-autonomous requirement of the USP/EcR-B ecdysone receptor for mushroom body neuronal remodeling in Drosophila. *Neuron*. 28:807–818. https://doi.org/10.1016/S0896-6273(00)00155-0

Lee, G., Z. Wang, R. Sehgal, C.-H. Chen, K. Kikuno, B. Hay, and J.H. Park. 2011. Drosophila caspases involved in developmentally regulated programmed cell death of peptidergic neurons during early metamorphosis. *J. Comp. Neurol.* 519:34–48. https://doi.org/10.1002/cne.22498

Lee, G., R. Sehgal, Z. Wang, S. Nair, K. Kikuno, C.-H. Chen, B. Hay, and J.H. Park. 2013. Essential role of grim-led programmed cell death for the establishment of corazonin-producing peptidergic nervous system during embryogenesis and metamorphosis in Drosophila melanogaster. *Biol. Open*. 2:283–294. https://doi.org/10.1242/bio.20133384

Lee, G., R. Sehgal, Z. Wang and J.H. Park. 2019. Ultraspiracle-independent anti-apoptotic function of ecdysone receptors is required for the survival of larval peptidergic neurons via suppression of grim expression in Drosophila melanogaster. *Apoptosis*. 24:256–268. https://doi.org/10.1007/s10495-019-01514-2

Lin, L., F.S.L.M. Rodrigues, C. Kary, A. Contet, M. Logan, R.H.G. Baxter, W. Wood, and E.H. Baehrecke. 2017. Complement-related regulates autophagy in neighboring cells. *Cell*. 170:158–171.e8. https://doi.org/10.1016/j.cell.2017.06.018

Luo, L., and D.D. O'Leary. 2005. Axon retraction and degeneration in development and disease. *Annu. Rev. Neurosci.* 28:127–156. https://doi.org/10.1146/annurev.neuro.28.061604.135632

Ma, Z., T. Stork, D.E. Bergles, and M.R. Freeman. 2016. Neuromodulators signal through astrocytes to alter neural circuit activity and behaviour. *Nature*. 539:428–432. https://doi.org/10.1038/nature20145

MacDonald, J.M., M.G. Beach, E. Porpiglia, A.E. Sheehan, R.J. Watts, and M.R. Freeman. 2006. The Drosophila cell corpse engulfment receptor Draper mediates glial clearance of severed axons. *Neuron*. 50:869–881. https://doi.org/10.1016/j.neuron.2006.04.028

Mack, T.G., M. Reiner, B. Beirowski, W. Mi, M. Emanuelli, D. Wagner, D. Thomson, T. Gillingwater, F. Court, L. Conforti, et al. 2001. Wallerian degeneration of injured axons and synapses is delayed by a Ube4b/Nmnat chimeric gene. *Nat. Neurosci.* 4:1199–1206. https://doi.org/10.1038/nn770

Manoukian, A.S., and H.M. Krause. 1992. Concentration-dependent activities of the even-skipped protein in Drosophila embryos. *Genes Dev.* 6:1740–1751. https://doi.org/10.1101/gad.6.9.1740

Marchetti, G., and G. Tavosanis. 2017. Steroid hormone ecdysone signaling specifies mushroom body neuron sequential fate via chinmo. *Curr. Biol.* 27:3017–3024.e4. https://doi.org/10.1016/j.cub.2017.08.037

Marín-Teva, J.L., I. Dusart, C. Colin, A. Gervais, N. van Rooijen, and M. Mallat. 2004. Microglia promote the death of developing Purkinje cells. *Neuron*. 41:535–547. https://doi.org/10.1016/S0896-6273(04)00069-8

Mayseless, O., G. Shapira, E.Y. Rachad, A. Fiala, and O. Schuldiner. 2023. Neuronal excitability as a regulator of circuit remodeling. *Curr. Biol.* 33:981–989.e3. https://doi.org/10.1016/j.cub.2023.01.032

Meltzer, H., E. Marom, I. Alyagor, O. Mayseless, V. Berkun, N. Segal-Gilboa, T. Unger, D. Luginbuhl, and O. Schuldiner. 2019. Tissue-specific (ts) CRISPR as an efficient strategy for in vivo screening in Drosophila. *Nat. Commun.* 10:2113. https://doi.org/10.1038/s41467-019-10140-0

Monedero Cobeta, I., B.Y. Salmani, and S. Thor. 2017. Anterior-Posterior gradient in neural stem and daughter cell proliferation governed by spatial and temporal hox control. *Curr. Biol.* 27:1161–1172. https://doi.org/10.1016/j.cub.2017.03.023

Neniskyte, U., and C.T. Gross. 2017. Errant gardeners: Glial-cell-dependent synaptic pruning and neurodevelopmental disorders. *Nat. Rev. Neurosci.* 18:658–670. https://doi.org/10.1038/nrn.2017.110

Nern, A., B.D. Pfeiffer, and G.M. Rubin. 2015. Optimized tools for multicolor stochastic labeling reveal diverse stereotyped cell arrangements in the fly visual system. *Proc. Natl. Acad. Sci. USA*. 112:E2967–E2976. https://doi.org/10.1073/pnas.1506763112

Neukomm, L.J., and M.R. Freeman. 2014. Diverse cellular and molecular modes of axon degeneration. *Trends Cell Biol.* 24:515–523. https://doi.org/10.1016/j.tcb.2014.04.003

Oppenheim, R.W. 1985. Naturally occurring cell death during neural development. *Trends Neurosci.* 8:487–493. https://doi.org/10.1016/0166-2236(85)90175-4

Perron, C., P. Carme, A.L. Rosell, E. Minnaert, S. Ruiz-Demoulin, H. Szczkowski, L.J. Neukomm, J.-M. Dura, and A. Boulanger. 2023. Chemokine-like Orion is involved in the transformation of glial cells into phagocytes in different developmental neuronal remodeling paradigms. *Development*. 150:dev201633. https://doi.org/10.1242/dev.201633

Petersen, C.C.H. 2019. Sensorimotor processing in the rodent barrel cortex. *Nat. Rev. Neurosci.* 20:533–546. https://doi.org/10.1038/s41583-019-0200-y

Pfeiffer, B.D., A. Jenett, A.S. Hammonds, T.-T.B. Ngo, S. Misra, C. Murphy, A. Scully, J.W. Carlson, K.H. Wan, T.R. Laverty, et al. 2008. Tools for neuroanatomy and neurogenetics in Drosophila. *Proc. Natl. Acad. Sci. USA*. 105:9715–9720. https://doi.org/10.1073/pnas.0803697105

Pinto-Teixeira, F., N. Konstantinides and C. Desplan. 2016. Programmed cell death acts at different stages of Drosophila neurodevelopment to shape the central nervous system. *FEBS Lett.* 590:2435–2453. https://doi.org/10.1002/1873-3468.12298

Poe, A.R., L. Tang, B. Wang, Y. Li, M.L. Sapar, and C. Han. 2017. Dendritic space-filling requires a neuronal type-specific extracellular permissive signal in Drosophila. *Proc. Natl. Acad. Sci. USA*. 114:E8062–E8071. https://doi.org/10.1073/pnas.1707467114

Reddien, P.W., S. Cameron, and H.R. Horvitz. 2001. Phagocytosis promotes programmed cell death in C. elegans. *Nature*. 412:198–202. https://doi.org/10.1038/35084096

Riccomagno, M.M., and A.L. Kolodkin. 2015. Sculpting neural circuits by axon and dendrite pruning. *Annu. Rev. Cell Dev. Biol.* 31:779–805. https://doi.org/10.1146/annurev-cellbio-100913-013038

Riddiford, L.M., and J.W. Truman. 1993. Hormone receptors and the regulation of insect metamorphosis. *Receptor*. 3:203–209. https://doi.org/10.1093/icb/33.3.340

Schafer, D.P., E.K. Lehrman, A.G. Kautzman, R. Koyama, A.R. Mardinly, R. Yamasaki, R.M. Ransohoff, M.E. Greenberg, B.A. Barres, and B. Stevens. 2012. Microglia sculpt postnatal neural circuits in an activity and complement-dependent manner. *Neuron*. 74:691–705. https://doi.org/10.1016/j.neuron.2012.03.026

Schindelin, J., I. Arganda-Carreras, E. Frise, V. Kaynig, M. Longair, T. Pietzsch, S. Preibisch, C. Rueden, S. Saalfeld, B. Schmid, et al. 2012. Fiji: An open-source platform for biological-image analysis. *Nat. Methods*. 9:676–682. https://doi.org/10.1038/nmeth.2019

Schubiger, M., A.A. Wade, G.E. Carney, J.W. Truman, and M. Bender. 1998. Drosophila EcR-B ecdysone receptor isoforms are required for larval molting and for neuron remodeling during metamorphosis. *Development*. 125:2053–2062. https://doi.org/10.1242/dev.125.11.2053

Schubiger, M., S. Tomita, C. Sung, S. Robinow, and J.W. Truman. 2003. Isoform specific control of gene activity in vivo by the Drosophila ecdysone receptor. *Mech. Dev.* 120:909–918. https://doi.org/10.1016/S0925-4773(03)00134-5

Sekar, A., A.R. Bialas, H. de Rivera, A. Davis, T.R. Hammond, N. Kamitaki, K. Tooley, J. Presumey, M. Baum, V. Van Doren, et al. 2016. Schizophrenia risk from complex variation of complement component 4. *Nature*. 530:177–183. https://doi.org/10.1038/nature16549

Selemon, L.D., G. Rajkowska, and P.S. Goldman-Rakic. 1995. Abnormally high neuronal density in the schizophrenic cortex. A morphometric analysis of prefrontal area 9 and occipital area 17. *Arch. Gen. Psychiatry*. 52:805–818; discussion 819–820. https://doi.org/10.1001/archpsyc.1995.03950220015005

Southwell, D.G., M.F. Paredes, R.P. Galvao, D.L. Jones, R.C. Froemke, J.Y. Sebe, C. Alfaro-Cervello, Y. Tang, J.M. Garcia-Verdugo, J.L. Rubenstein, et al. 2012. Intrinsically determined cell death of developing cortical interneurons. *Nature*. 491:109–113. https://doi.org/10.1038/nature11523

Stevens, B., N.J. Allen, L.E. Vazquez, G.R. Howell, K.S. Christopherson, N. Nouri, K.D. Micheva, A.K. Mehalow, A.D. Huberman, B. Stafford, et al. 2007. The classical complement cascade mediates CNS synapse elimination. *Cell*. 131:1164–1178. https://doi.org/10.1016/j.cell.2007.10.036

Talbot, W.S., E.A. Swyryd, and D.S. Hogness. 1993. Drosophila tissues with different metamorphic responses to ecdysone express different ecdysone receptor isoforms. *Cell*. 73:1323–1337. https://doi.org/10.1016/0092-8674(93)90359-X

Tasdemir-Yilmaz, O.E., and M.R. Freeman. 2014. Astrocytes engage unique molecular programs to engulf pruned neuronal debris from distinct subsets of neurons. *Genes Dev.* 28:20–33. https://doi.org/10.1101/gad.229518.113

Thummel, C.S. 1996. Flies on steroids--Drosophila metamorphosis and the mechanisms of steroid hormone action. *Trends Genet.* 12:306–310. https://doi.org/10.1016/0168-9525(96)10032-9

Truman, J.W., W.S. Talbot, S.E. Fahrbach, and D.S. Hogness. 1994. Ecdysone receptor expression in the CNS correlates with stage-specific responses to ecdysteroids during Drosophila and Manduca development. *Development*. 120:219–234. https://doi.org/10.1242/dev.120.1.219

Viswanathan, S., M.E. Williams, E.B. Bloss, T.J. Stasevich, C.M. Speer, A. Nern, B.D. Pfeiffer, B.M. Hooks, W.-P. Li, B.P. English, et al. 2015. High-performance probes for light and electron microscopy. *Nat. Methods*. 12:568–576. https://doi.org/10.1038/nmeth.3365

Wang, Z., G. Lee, R. Vuong, and J.H. Park. 2019. Two-factor specification of apoptosis: TGF-β signaling acts cooperatively with ecdysone signaling to induce cell- and stage-specific apoptosis of larval neurons during metamorphosis in Drosophila melanogaster. *Apoptosis*. 24:972–989. https://doi.org/10.1007/s10495-019-01574-4

Watts, R.J., E.D. Hoopfer, and L. Luo. 2003. Axon pruning during Drosophila metamorphosis: Evidence for local degeneration and requirement of the ubiquitin-proteasome system. *Neuron*. 38:871–885. https://doi.org/10.1016/S0896-6273(03)00295-2

Williams, D.W., and J.W. Truman. 2005. Cellular mechanisms of dendrite pruning in Drosophila: Insights from in vivo time-lapse of remodeling dendritic arborizing sensory neurons. *Development*. 132:3631–3642. https://doi.org/10.1242/dev.01928

Winbush, A., and J.C. Weeks. 2011. Steroid-triggered, cell-autonomous death of a Drosophila motoneuron during metamorphosis. *Neural Dev.* 6:15. https://doi.org/10.1186/1749-8104-6-15

Winchester, C.L., H. Ohzeki, D.A. Vouyiouklis, R. Thompson, J.M. Penninger, K. Yamagami, J.D. Norrie, R. Hunter, J.A. Pratt, and B.J. Morris. 2012. Converging evidence that sequence variations in the novel candidate gene MAP2K7 (MKK7) are functionally associated with schizophrenia. *Hum. Mol. Genet.* 21:4910–4921. https://doi.org/10.1093/hmg/dds331

Yamaguchi, Y., and M. Miura. 2015. Programmed cell death in neurodevelopment. *Dev. Cell*. 32:478–490. https://doi.org/10.1016/j.devcel.2015.01.019

Yaniv, S.P., and O. Schuldiner. 2016. A fly's view of neuronal remodeling. *Wiley Interdiscip. Rev. Dev. Biol.* 5:618–635. https://doi.org/10.1002/wdev.241

Yao, T.P., B.M. Forman, Z. Jiang, L. Cherbas, J.D. Chen, M. McKeown, P. Cherbas, and R.M. Evans. 1993. Functional ecdysone receptor is the product of EcR and Ultraspiracle genes. *Nature*. 366:476–479. https://doi.org/10.1038/366476a0

Yu, X.M., I. Gutman, T.J. Mosca, T. Iram, E. Ozkan, K.C. Garcia, L. Luo, and O. Schuldiner. 2013. Plum, an immunoglobulin superfamily protein, regulates axon pruning by facilitating TGF-β signaling. *Neuron*. 78:456–468. https://doi.org/10.1016/j.neuron.2013.03.004

Yunsik, K., J. Amanda, S. Amy, D.L.T. Rachel, J. Taylor, C. Lucia, H. Alex, C. Megan, B. Isabelle, Z. Zheng, and R.F. Marc. 2023. Tweek-dependent formation of ER-PM contact sites enables astrocyte phagocytic function and remodeling of neurons. *bioRxiv*. https://doi.org/10.1101/2023.11.06.565932 (Preprint posted November 07, 2023).

Zhang, H., Y. Wang, J.J. Wong, K.L. Lim, Y.C. Liou, H. Wang, and F. Yu. 2014. Endocytic pathways downregulate the L1-type cell adhesion molecule neuroglian to promote dendrite pruning in Drosophila. *Dev. Cell*. 30:463–478. https://doi.org/10.1016/j.devcel.2014.06.014

Zheng, X., J. Wang, T.E. Haerry, A.Y.H. Wu, J. Martin, M.B. O'Connor, C.-H.J. Lee, and T. Lee. 2003. TGF-β signaling activates steroid hormone receptor expression during neuronal remodeling in the Drosophila brain. *Cell*. 112:303–315. https://doi.org/10.1016/S0092-8674(03)00072-2

Zhu, S., R. Chen, P. Soba, and Y.-N. Jan. 2019. JNK signaling coordinates with ecdysone signaling to promote pruning of Drosophila sensory neuron dendrites. *Development*. 146:dev163592. https://doi.org/10.1242/dev.163592

Zirin, J., D. Cheng, N. Dhanyasi, J. Cho, J.-M. Dura, K. Vijayraghavan, and N. Perrimon. 2013. Ecdysone signaling at metamorphosis triggers apoptosis of Drosophila abdominal muscles. *Dev. Biol.* 383:275–284. https://doi.org/10.1016/j.ydbio.2013.08.029

Supplemental material

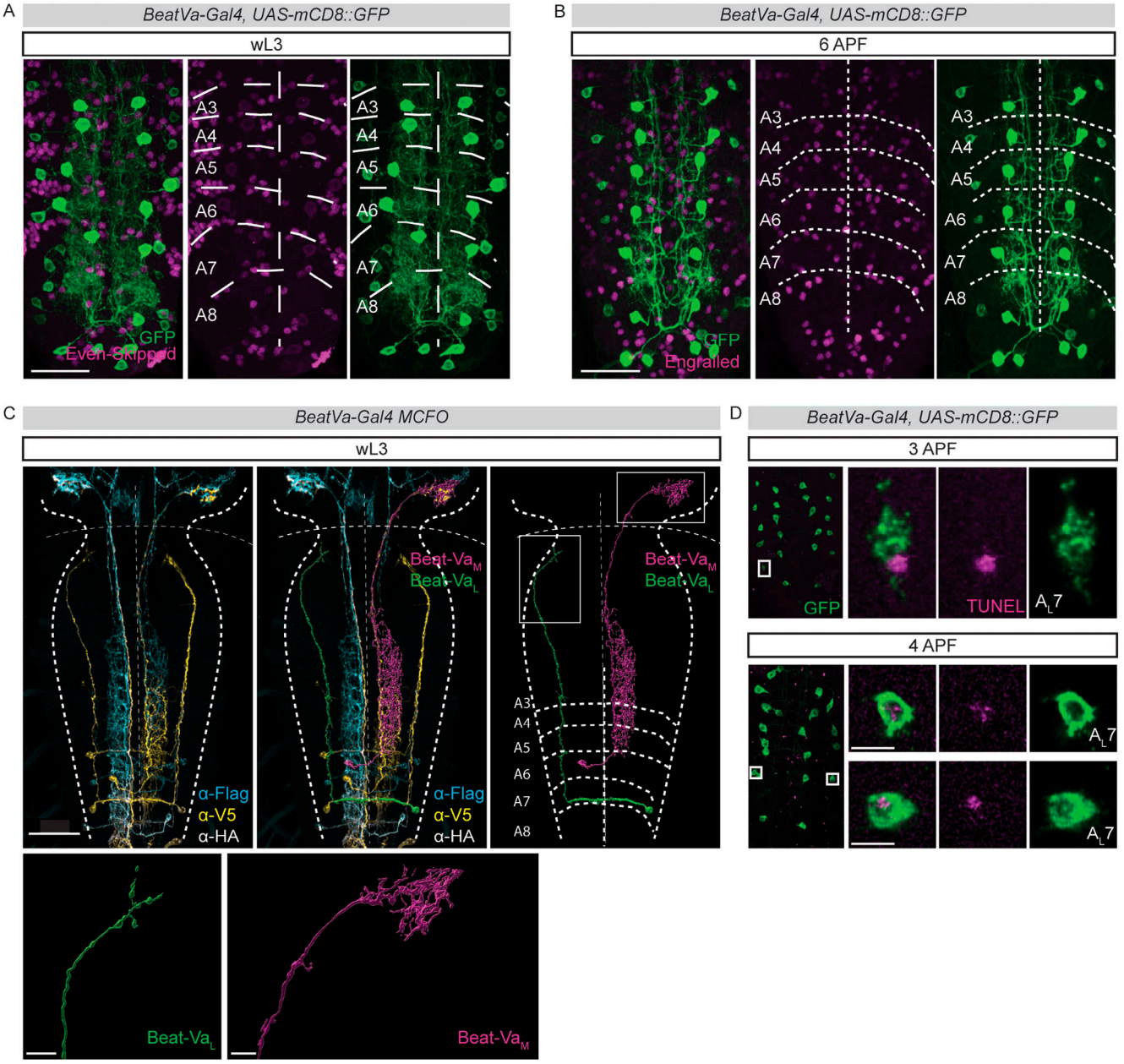

Figure S1. **Segmental characterization of Beat-Va$_M$ and Beat-Va$_L$ neurons. (A)** VNC at wL3 with genetic mCD8::GFP labeling of Beat-Va neurons (green) and anti-Even-Skipped staining (magenta) to label the segments of the ventral nerve cord. Segments A3–A8 are denoted by tracing the Even-Skipped staining and then superimposed onto Beat-Va neurons to define segmental positions. Scale bar is 20 µm. **(B)** VNC at 6 h APF with genetic GFP labeling of Beat-Va neurons (green) and anti-Engrailed staining (magenta) to label the segments of the VNC, showing the segmental positions persist into metamorphosis. Scale bars are 20 µm. **(C)** Using segmental information and MCFO we can render single cells in Imaris and overlay positional information. Boxed areas are Beat-Va$_L$ and Beat-Va$_M$ termini and are displayed in high magnification (scale bars are 10 µm). CNS is outlined and boundary between VNC and brain lobes is marked with a dashed line. **(D)** Z-projection of ventral nerve cords with Beat-Va neurons labeled genetically with mCD8::GFP (green) and then subjected to TUNEL staining (magenta) to detect cells undergoing apoptotic cell death at 3 h APF and 4 h APF. Boxed areas containing TUNEL-positive lateral cells are magnified and segmental position is noted. Scale bar is 5 µm.

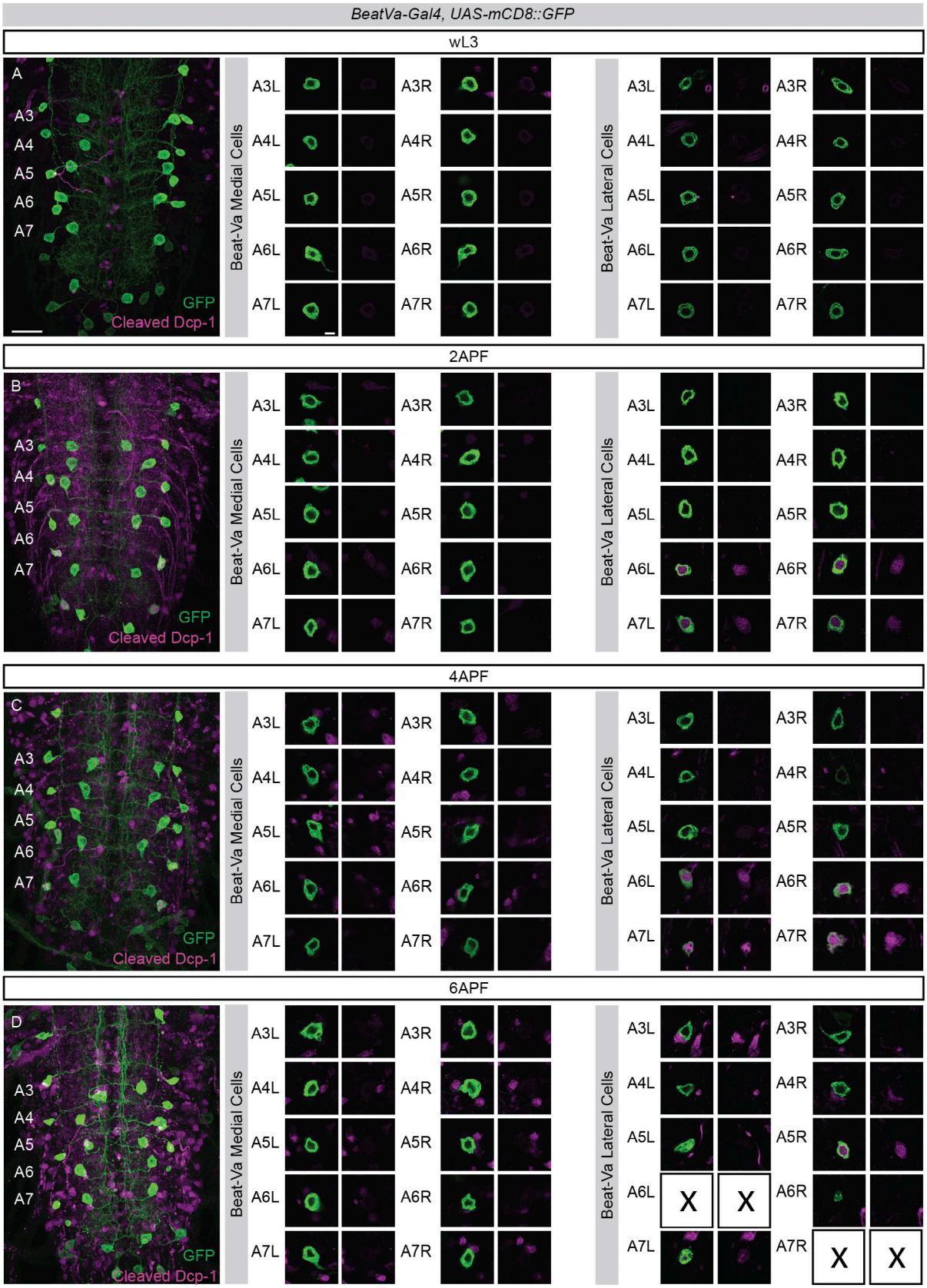

Figure S2. **Beat-Va$_L$ but not Beat-Va$_M$ neurons display caspase activation during metamorphosis. (A–D)** Beat-Va neurons genetically labeled with mCD8::GFP and stained for cleaved Dcp-1 at wL3 (A), 2 h APF (B), 4 h APF (C), or 6 h APF (D). Right, A3–A7 lateral and medial cells from each hemisegment (L = left and R = right hemisegment) are magnified and shown as a single plane image on the right of each full VNC image. Scale bars are 20 µm in population images and 5 µm in the magnified view.

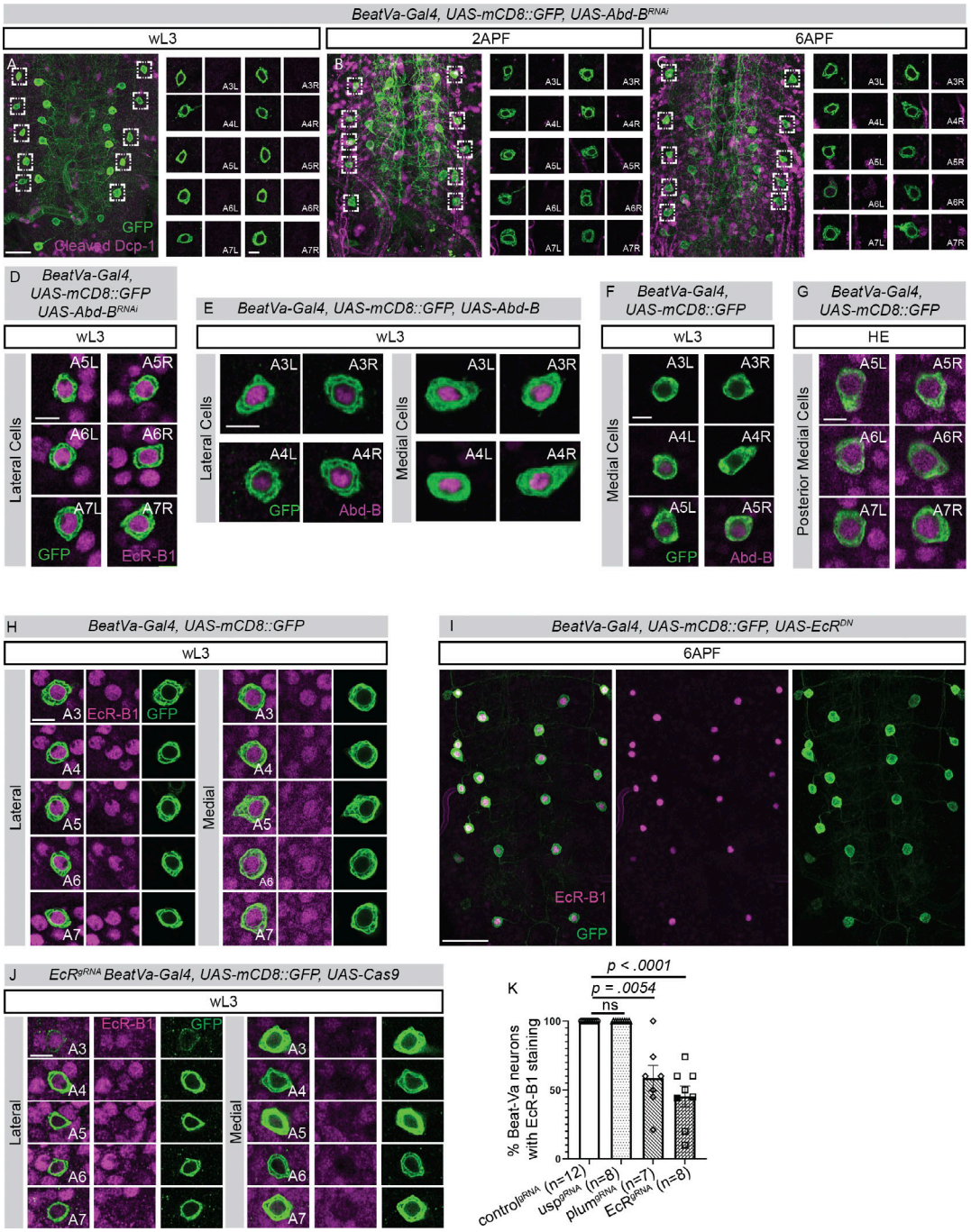

Figure S3. **Abd-B and EcR signaling drive Beat-Va$_L$ cell death but not Beat-Va$_M$ remodeling. (A–C)** Beat-Va neurons genetically labeled with mCD8::GFP and driving a *UAS-Abd-B^{RNAi}* at wL3 (A), 2 h APF (B), and 6 h APF (C) stained for cleaved Dcp-1. Magnified views of A3–A7 lateral cells from the right and left are shown as a single plane image on the right of each image. **(D)** Beat-Va neurons labeled with mCD8::GFP and driving *UAS-Abd-B^{RNAi}* at wL3 stained with the EcR-B1 showing the continued colocalization of EcR-B1 in the absence of Abd-B. **(E)** Beat-Va neurons at wL3 genetically labeled with mCD8::GFP and crossed to *UAS-Abd-B* and stained with anti-Abd-B. The two most anterior lateral and medial cell bodies are magnified and show Abd-B expression, which is not usually present in these cells, confirming overexpression was successful. **(F)** The three most anterior medial Beat-Va neurons at wL3 labeled with CD8::GFP and stained with Abd-B shows Abd-B is present in some medial cells even though they do not undergo cell death. **(G)** Beat-Va$_M$ neurons at HE genetically labeled with mCD8::GFP and stained with anti-Abd-B. The A5–7 medial cells continue to express Abd-B at HE. Left and right hemisegment denoted by "L" and "R." **(H)** Beat-Va neurons at wL3 genetically labeled CD8::GFP (green) stained with the EcR-B1 Receptor (magenta) showing all lateral and medial cell bodies express the receptor. **(I)** Beat-Va neurons at 6 h APF genetically labeled with CD8::GFP (green), expressing a UAS regulated EcR^{DN}, and stained with the EcR-B1 Receptor (magenta) to identify cells that express *UAS-EcR^{DN}*. There are typically no EcR-B1 positive cells at this time. **(J)** Beat-Va neurons at wL3 genetically labeled CD8::GFP (green) and expressing *UAS-Cas9* and EcR-targeting gRNA ubiquitously. Stained with the EcR-B1 Receptor (magenta) to evaluate if cells lose EcR-B1 expression. **(K)** Quantification of gRNA against *usp*, *plum*, *EcR* on Beat-Va EcR-B1 expression when compared with control. One-way ANOVA, Kruskal–Wallis test for multiple comparisons. *n* = number of animals. Colored data points correspond to the representative image shown in the figure. All error bars are SEM. Scale bar is 5 µm in all images with a single cell body and 20 µm in all other images.

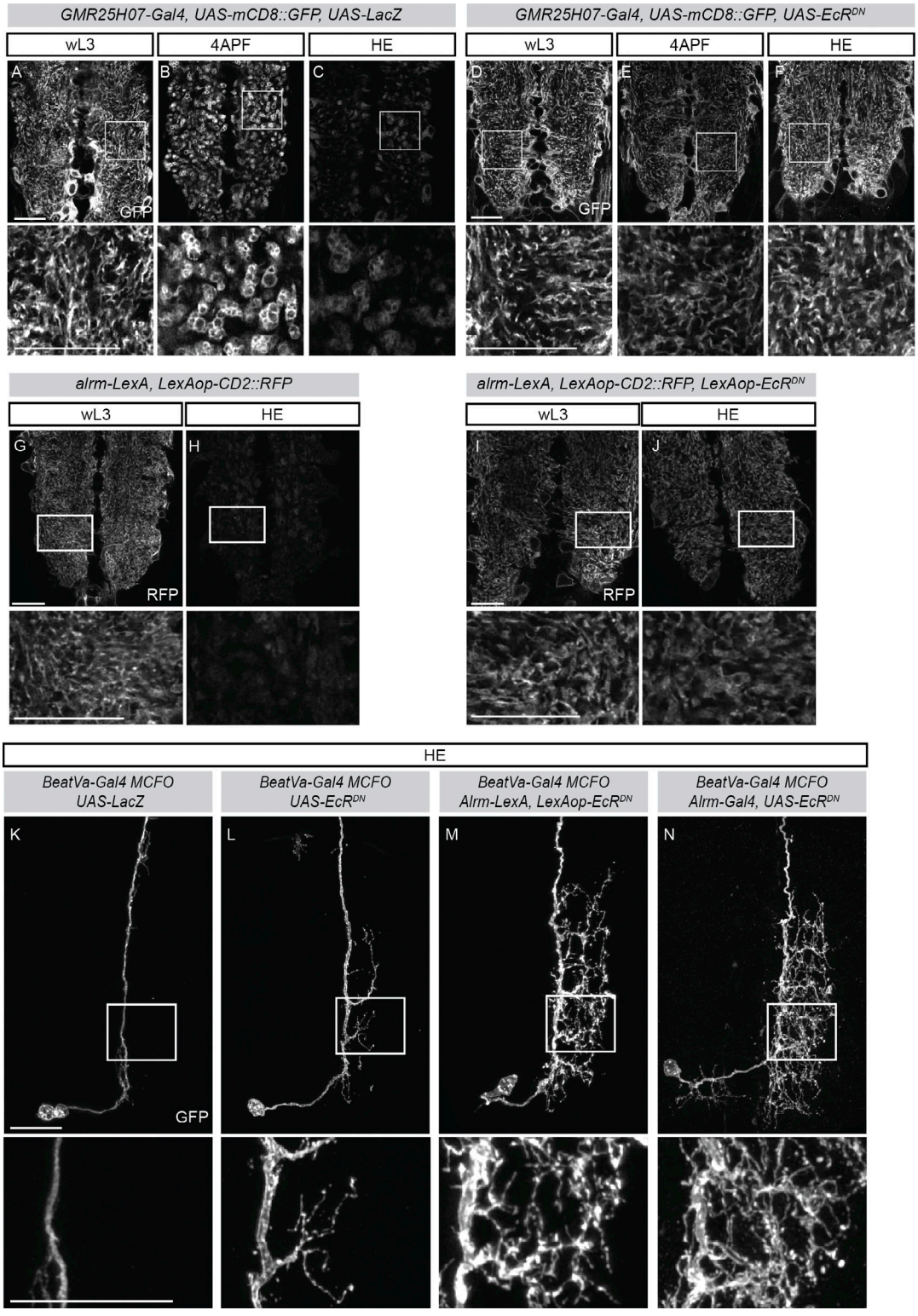

Figure S4. **Cell autonomous expression of EcR^{DN} blocks astrocyte transformation and has additive effects in Beat-Va neurite pruning. (A–C)** Astrocytes genetically manipulated with *GMR25H07-Gal4* (a strong astrocyte Gal4 line) crossed to UAS-CD8::GFP (A) show a "wispy" morphology at wL3, (B) display many phagolysomes at 4 h APF (Yunsik et al., 2023, *Preprint*), and (C) are normally only faintly detectable by HE. **(D–F)** Astrocytes expressing a *UAS-EcR^{DN}*, labeled with mCD8::GFP at wL3 (D) showing their "wispy" morphology, which is retained at (E) 4 h APF, and (F) HE, indicating a failure to transform. **(G and H)** *arm-LexA, LexAop-mCD8::RFP* at (G) wL3 where normal astrocyte morphology is apparent, and (H) HE when astrocytes are no longer visible. **(I and J)** (I) When *alrm-LexA* drives a *LexAop-EcR^{DN}* in addition to *LexAop-mCD8::RFP*, astrocytes appear normal at wL3, (J) but then fail to transform at HE. Scale bars are 20 µm. **(K–N)** (K) Micrograph of a single cell MFCO clones at HE in the control condition, (L) when EcR^{DN} is expressed only in Beat-Va neurons, (M) when astrocyte transformation is blocked via astrocytic expression of EcR, and (N) when both neuronal and astrocytic EcR signaling is blocked. All scale bars are 20 µm.

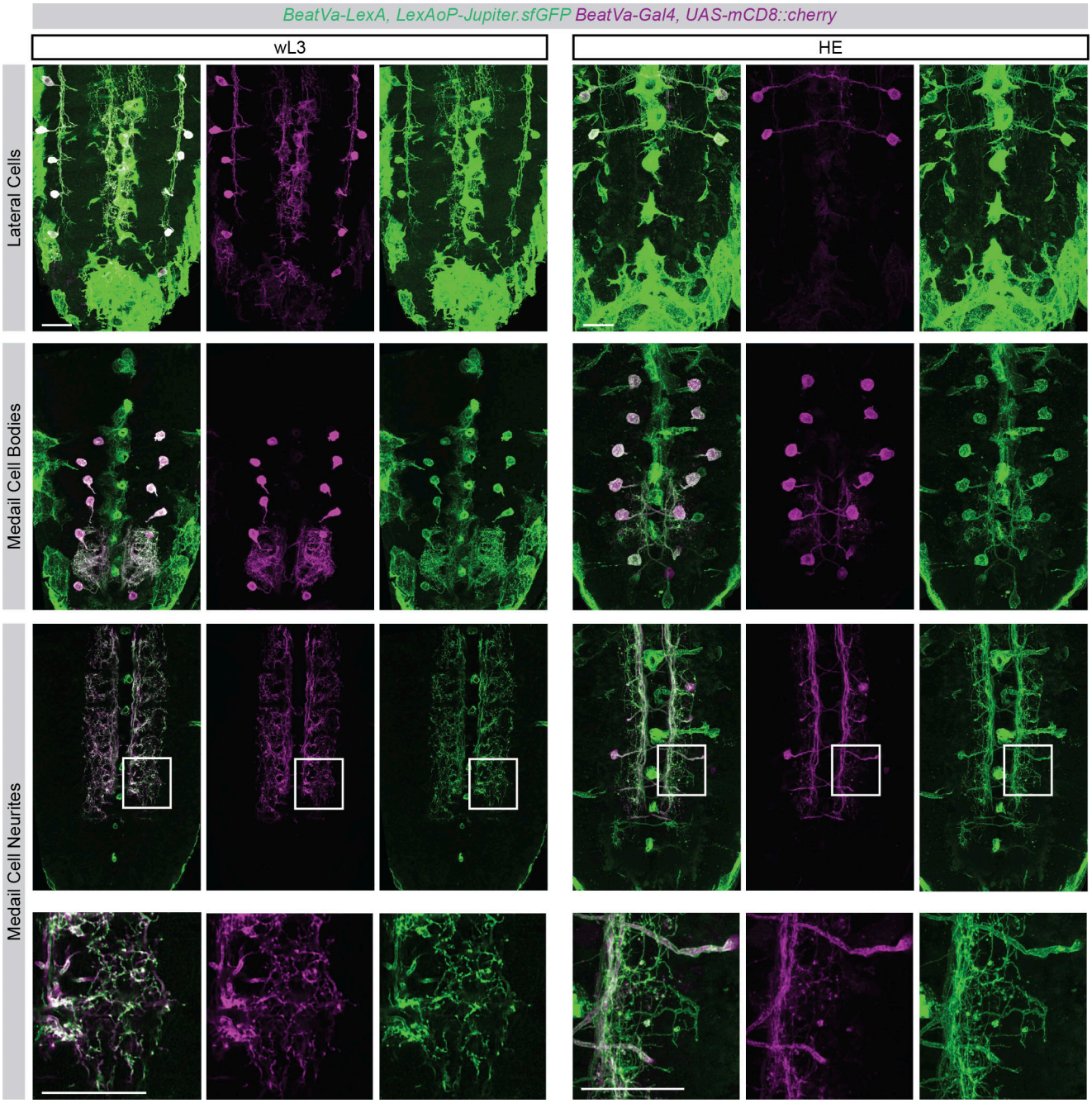

Figure S5. **Verification of newly constructed *BeatVa-LexA* line.** Animals carrying the *BeatVa-LexA* construct were crossed to animals carrying a *LexAop-Jupiter.sfGFP* (a GFP construct that localizes to microtubule networks and has been reported to label neurite processes well [Karpova et al., 2006]) to genetically label any cells where the *BeatVa-LexA* line was expressed. These animals were then crossed to an existing stock that carried both the original *BeatVa-Gal4* construct and a *UAS-mCD8::cherry*. Good signal overlap between the GFP and Cherry fluorophores indicates the *BeatVa-LexA* and *BeatVa-Gal4* lines labeled the same population of neurons in addtion to labeling a second population of non-neuronal cells (likely surface glia). Scale bars are 20 µm.

Provided online are Table S1, Table S2, Table S3, and Table S4. Table S1 shows in vivo evaluation of *Gal4* lines at wL3. Table S2 shows in vivo evaluation of Gal4 lines for sparse neuronal labeling at multiple time points. Table S3 shows targeted screen to find genes that drive astrocyte mediated Beat-Va$_M$ neuronal remodeling. Table S4 is a resource table.